Title

Cross-species genomics reveals oncogenic dependencies in ZFTA/C11orf95 fusion-positive supratentorial ependymomas

Authors/Affiliations

Tuyu Zheng[1,2,3,38], David R. Ghasemi[1,2,38], Konstantin Okonechnikov[1,2,38], Andrey Korshunov[1,4,5], Martin Sill[1,2], Kendra K. Maass[1,2,6], Patricia Benites Goncalves da Silva[1,2], Marina Ryzhova[7], Johannes Gojo[1,8], Damian Stichel[4,5], Amir Arabzade[9,10], Robert Kupp[11], Julia Benzel[1,2,3], Shinichiro Taya[12], Toma Adachi[12], Ryo Shiraishi[12], Nicolas U. Gerber[13], Dominik Sturm[1,6,14], Jonas Ecker[1,6,15], Philipp Sievers[4,5], Florian Selt[1,6,15], Rebecca Chapman[16], Christine Haberler[17], Dominique Figarella-Branger[18], Guido Reifenberger[19,20], Gudrun Fleischhack[21], Stefan Rutkowski[22], Andrew M. Donson[23], Vijay Ramaswamy[24], David Capper[25,26], David W. Ellison[27], Christel C. Herold-Mende[28], Ulrich Schüller[22,29,30], Sebastian Brandner[31,32], Pablo Hernáiz Driever[33], Johan M. Kros[34], Matija Snuderl[35], Till Milde[1,6,15], Richard G. Grundy[16], Mikio Hoshino[12], Stephen C. Mack[9], Richard J. Gilbertson[11,36], David T.W. Jones[1,14], Marcel Kool[1,2,37], Andreas von Deimling[4,5], Stefan M. Pfister[1,2,6], Felix Sahm[1,4,5,39], Daisuke Kawauchi[1,2,12,39], Kristian W. Pajtler[1,2,6,39]

Author List Footnotes

1) Hopp Children's Cancer Center Heidelberg (KiTZ), 69120 Heidelberg, Germany.
2) Division of Pediatric Neurooncology, German Cancer Research Center (DKFZ) and German Cancer Consortium (DKTK), 69120 Heidelberg, Germany.
3) Faculty of Biosciences, Heidelberg University, 69117 Heidelberg, Germany
4) Clinical Cooperation Unit Neuropathology, German Cancer Research Center (DKFZ), 69120 Heidelberg, Germany.
5) Department of Neuropathology, Heidelberg University Hospital, 69120 Heidelberg, Germany.
6) Department of Pediatric Oncology, Hematology, and Immunology, University Hospital Heidelberg, Heidelberg, Germany.
7) Department of Neuropathology, NN Burdenko Neurosurgical Institute, 125047 Moscow, Russia.
8) Department of Pediatrics and Adolescent Medicine and Comprehensive Center for Pediatrics, Medical University of Vienna, Vienna, Austria.
9) Department of Pediatrics, Division of Hematology and Oncology, Baylor College of Medicine, Texas Children's Hospital, Houston, TX 77030, USA.
10) Department of Chemical and Biomolecular Engineering, Rice University, Houston TX, USA.
11) Cancer Research UK Cambridge Institute, University of Cambridge, Li Ka Shing Centre, Robinson Way, Cambridge CB2 0RE, England.
12) Department of Biochemistry and Cellular Biology, National Institute of Neuroscience, NCNP, Tokyo, 187-0031, Japan.

13) Department of Oncology, University Children's Hospital, Zurich, Switzerland.
14) Pediatric Glioma Research Group, German Cancer Research Center (DKFZ), Heidelberg, Germany.
15) Clinical Cooperation Unit Pediatric Oncology, German Cancer Research Center (DKFZ) and German Consortium for Translational Cancer Research (DKTK), Heidelberg, Germany.
16) Children's Brain Tumour Research Centre, School of Medicine, University of Nottingham, Nottingham, UK.
17) Division of Neuropathology and Neurochemistry, Department of Neurology, Medical University of Vienna.
18) Department of Pathology and Neuropathology, La Timone Hospital, Aix Marseille University, Marseille, France.
19) Institute of Neuropathology, Heinrich Heine University, Medical Faculty, Duesseldorf, Germany.
20) German Cancer Consortium (DKTK), Partner Site Essen/Duesseldorf, Germany.
21) Pediatric Oncology and Hematology, Pediatrics III, University Hospital of Essen, Essen, Germany.
22) Department of Paediatric Haematology and Oncology, University Medical Center Hamburg-Eppendorf, Hamburg, Germany.
23) University of Colorado Anschutz Medical Campus, Aurora, CO 80045, USA.
24) Department of Paediatrics, The Hospital for Sick Children, Toronto, Ontario, Canada.
25) Department of Neuropathology, Charité - Universitätsmedizin Berlin, corporate member of Freie Universität Berlin, Humboldt-Universität zu Berlin, and Berlin Institute of Health, Berlin, Germany.
26) German Cancer Consortium (DKTK), Partner Site Berlin, German Cancer Research Center (DKFZ), Heidelberg, Germany.
27) Department of Pathology, St Jude Children's Research Hospital, Memphis, TN, USA.
28) Department of Neurosurgery, Heidelberg University Hospital, Heidelberg, Germany.
29) Research Institute, Children's Cancer Center Hamburg, Hamburg, Germany.
30) Institute of Neuropathology, University Medical Center Hamburg-Eppendorf, Hamburg, Germany.
31) Division of Neuropathology, UCL Queen Square Institute of Neurology and The National Hospital for Neurology and Neurosurgery, University College London Hospitals NHS Foundation Trust.
32) Department of Neurodegenerative Disease, UCL Queen Square Institute of Neurology, Queen Square, London WC1N 3BG, UK.
33) Department of Pediatric Oncology/Hematology, Charité - Universitätsmedizin Berlin, Corporate Member of Freie Universität Berlin, Humboldt-Universität zu Berlin, and Berlin Institute of Health, Berlin, Germany.
34) Department of Pathology, Erasmus University Medical Center, Rotterdam, The Netherlands.
35) Division of Neuropathology, Department of Pathology, NYU Langone Health, New York, New York, USA.
36) Department of Oncology, University of Cambridge, Hutchison/MRC Research Centre, Box 197, Cambridge Biomedical Campus, Cambridge CB2 0XZ, England.
37) Princess Máxima Centre for Paediatric Oncology, Utrecht, Netherlands.
38) These authors contributed equally to this study.
39) These authors jointly supervised this study.

Running title

ZFTA fusion genes in supratentorial ependymomas

Keywords

Ependymoma, fusion oncoprotein, ZFTA, C11orf95, RELA, GLI2

Corresponding Authors:
Kristian W. Pajtler, MD, MBA (K.W.P.)
Hopp Children's Cancer Center Heidelberg (KiTZ),
Division of Pediatric Neurooncology, German Cancer Research Center (DKFZ) and German Cancer Consortium (DKTK),
Department of Pediatric Oncology, Hematology, and Immunology, University Hospital Heidelberg, Heidelberg, Germany
Im Neuenheimer Feld 580
69120 Heidelberg
Germany
Phone: +496221424585
k.pajtler@kitz-heidelberg.de

Daisuke Kawauychi, Ph.D (D.K.)
National Center of Neurology and Psychiatry (NCNP)
Institute of Neuroscience
Department of Biochemistry and Cellular Biology
4-1-1 Ogawahigashi-machi,
Kodaira, Tokyo, 187-0031, JAPAN
Phone: +81-42-346-1722
d.kawauchi@ncnp.go.jp

Felix Sahm, MD, PhD (F.S.)
Department of Neuropathology
University Hospital Heidelberg
and
Clinical Cooperation Unit Neuropathology (B300)
German Cancer Research Center (DKFZ)
and
Hopp Children's Cancer Center Heidelberg (KiTZ),
Im Neuenheimer Feld 224
69120 Heidelberg, Germany
Phone: +49-6221 56-37886; Fax: +49-6221 56 4566
felix.sahm@med.uni-heidelberg.de

Disclosure of Potential Conflicts of Interest

The authors declare no conflict of interest.

Abstract

Molecular groups of supratentorial ependymomas comprise tumors with *ZFTA-RELA* or *YAP1*-involving fusions and fusion-negative subependymoma. However, occasionally supratentorial ependymomas cannot be readily assigned to any of these groups due to lack of detection of a typical fusion and/or ambiguous DNA methylation-based classification. An unbiased approach with a cohort of unprecedented size revealed distinct methylation clusters composed of tumors with ependymal but also various other histological features containing alternative translocations that shared *ZFTA* as a partner gene. Somatic overexpression of *ZFTA*-associated fusion genes in the developing cerebral cortex is capable of inducing tumor formation *in vivo*, and cross-species comparative analyses identified *GLI2* as a key downstream regulator of tumorigenesis in all tumors. Targeting GLI2 with arsenic trioxide caused extended survival of tumor-bearing animals, indicating a potential therapeutic vulnerability in ZFTA fusion-positive tumors. (Word count: 131)

Significance

ZFTA-RELA fusions are a hallmark feature of supratentorial ependymoma. We find that ZFTA acts as a partner for alternative transcriptional activators in oncogenic fusions of supratentorial tumors with various histological characteristics. Establishing representative mouse models, we identify potential therapeutic targets shared by *ZFTA* fusion-positive tumors, such as GLI2. (Word count: 48)

Introduction

Ependymomas (EPN) are neuroepithelial malignancies of the central nervous system (CNS), accounting for 5% of all CNS tumors in children (1). The utility of histological grading of EPN for risk stratification has been discussed controversially, with no consistent associations of tumor grade and patient outcome (2). However, recent genomic studies have allowed for subdivision of supratentorial (ST), posterior fossa (PF) and spinal (SP) EPN into molecularly distinct groups with clearly distinct clinical features and outcome (3-9). Despite these advances, translation into novel treatment approaches is lagging behind. The mainstay of treatment for almost all EPNs remains surgery and radiotherapy, whereas chemotherapy has mostly been found to be ineffective (10,11).

Within the ST CNS compartment, underlying molecular signatures including DNA methylation and transcriptome analysis define three major subgroups, designated ST-SE, ST-EPN-YAP1 and ST-EPN-RELA (6). ST-SE are fusion-negative molecularly classified subependymoma that are mostly observed in adults. ST-EPN-YAP1 tumors are enriched for gene fusions involving the Hippo effector *YAP1* and primarily affect infants. The vast majority of ST-EPN is classified best as ST-EPN-RELA and the tumors predominantly contain oncogenic fusions between *RELA*, the principal effector of canonical NF-κB signaling, and *C11orf95*, a less well characterized neighboring gene on chromosome (chr.) 11 (6,7,12).

Apart from chromothriptic events on chr. 11 surrounding the fusion, the genome of human ST-EPN-RELA is generally stable and additional recurrent alterations other than focal *CDKN2A/B* deletions have not yet been identified (6). The hypothesis of a single-hit oncogenic event is supported by the fact that the *C11orf95-RELA* fusion is sufficient to drive tumor formation *in vivo* using the RCAS/tv-a system (13). In ST-EPN-YAP1, MAMLD1 (the most frequent fusion partner to YAP1) was found to mediate fusion-driven oncogenic transformation of cortical neural progenitors through nuclear translocation and interaction with nuclear factor I proteins (14). The role of the RELA fusion partner C11orf95 in ST-EPN-RELA, however, is not yet fully understood. Results from previous studies show that overexpression of wild-type *RELA* or induction of activating *RELA* mutations are not sufficient for oncogenesis, despite leading to elevated levels of NF-κB target genes. This indicates that both the Rel-homology domain of RELA and the C11orf95 partner gene are critical for ependymal tumorigenesis (7,13).

Although ST-EPNs are mostly unambiguously assigned to a molecular group by the Heidelberg Brain Tumor Methylation Classifier (www.molecularneuropathology.org) (15), one of the following three diagnostically challenging constellations may occur in about 20% of all ST-EPN cases (12,16-19): (i) prediction as ST-EPN-RELA by DNA methylation-based tumor classification but without evidence for a canonical *C11orf95-RELA* fusion, (ii) the *vice versa* combination with a typical fusion event in the absence of a reliable ST-EPN-RELA score or (iii) ST tumors histologically diagnosed as EPN that cannot be readily assigned to any of the existing molecular classes. In this study, we aimed to molecularly characterize *RELA*- and *YAP1*-fusion negative ST-EPN tumors, which exist in addition to the known fusion-negative ST-SE group. We demonstrate the existence of both ST-EPN harboring *C11orf95* fusions to gene partners other than *RELA,* and ST tumors that are histologically distinct from EPN but harbor a canonical *C11orf95-RELA* fusion. In addition, we show that newly identified *C11orf95*-associated fusions possess transforming capacity *in vivo*. Our current study paves the way for a refined molecular classification of ST-EPN in the future, provides representative mouse models and presents a rationale for preclinical studies aiming at blocking central molecular dependencies and target genes (e.g., *GLI2*) that are shared by tumors driven by *C11orf95*-containing fusion genes independent of histological appearance. Based on our findings together with two co-submitted studies by Kupp et al. and Arabzade et al. (20,21), *C11orf95* has now been officially designated *ZFTA* (zinc finger translocation associated) by the HUGO Gene Nomenclature Committee.

Results

Diagnostically ambiguous supratentorial ependymomas form discrete clusters

To identify molecular group assignment of diagnostically challenging ST-EPN we included 23 samples fulfilling any of the conditions i-iii in an unbiased clustering approach with a comprehensive dataset of DNA methylation profiles covering the entire spectrum of existing molecular CNS tumor classes (>70,000 DNA methylation profiles) (Supplementary Fig. S1, S2A). Exploratory samples were mainly clustering in smaller satellite clusters next to (18/23) or within the ST-EPN-RELA cluster (2/23), 3/23 were not assigned to any cluster and excluded from further analysis (Supplementary Fig. S2A). Next, we restricted the clustering approach to cases from established

molecular EPN groups and satellites only, revealing four distinct additional clusters (Fig. 1A). Cluster stability was confirmed through a hierarchical density-based clustering scan (HDBSCAN) (Fig. 1B, Supplementary Fig. S2B and C, Supplementary Table S1). Tumors from the ST-EPN-RELA cluster (445/492; 90.4%) and cluster 1 (9/9; 100%) predominantly reached a calibrated score for reliable ST-EPN-RELA methylation group assignment by the Heidelberg Brain Tumor Methylation Classifier, score ≥0.9 (=red dots; classifier version 11b4) (Fig. 1B) (15). In cluster 2, only 22/43 (51.1%) reached a calibrated score ≥0.9 for ST-EPN-RELA. All samples of the two remaining clusters 3 and 4 (n=17, and n=27) were found unclassifiable with calibrated scores <0.9 for any methylation class (=black dots) (Fig. 1B, Supplementary Table S1). Control for potential confounding effects through tumor purity, array or tissue type and probe detection quality did not reveal significant impact by any of these factors (Supplementary Fig. S3A-F). Copy number alterations (CNA) previously described for ST-EPN-RELA, such as loss of *CDKN2A*, or chromothriptic events on chr. 11 were found to different extents. Loss of chr. 22 was associated with all clusters (Fig. 1C, Supplementary Table S2) (6,7). Notably, copy number alterations were calculated from Illumina 450k or Illumina 850k/EPIC arrays, and chromothriptic events may have been called more frequently applying whole-genome sequencing. Taken together, these data demonstrate that diagnostically challenging ST-EPNs (exploratory samples), i.e. unclassifiable tumors based on DNA methylation or without evidence for a typical fusion, mainly fall into discrete DNA methylation clusters distinct from ST-EPN-RELA and only partly share structural variations with these.

ST-EPN-RELA satellite clusters harbor alternative *ZFTA* fusion genes

Next, we further investigated molecular characteristics of satellite clusters 1 to 4 as compared to ST-EPN-RELA. To this end, we performed either RNA-sequencing or DNA panel-sequencing and also incorporated previously generated data (RNA-sequencing and RT-PCR), resulting in comprehensive fusion gene information from clusters 1-4 (n = 48) and ST-EPN-RELA samples (n = 70) (6,22)(Supplementary Table S1). Sequencing data revealed a previously unrecognized *ZFTA-RELA* fusion type in cluster 1 (n = 2/2), designated fusion type 8 (7) (Fig. 2A, B). All samples from cluster 3 subjected to DNA panel-sequencing (n = 5/13), RNA-sequencing (n = 6/13) or both methods (n = 2/13) harbored a *ZFTA-RELA* (type 1, 2 or 3) fusion (Fig. 2A and Supplementary Table S1) (7). Notably, samples from cluster 3 were invariably

unclassifiable (ST-EPN-RELA score < 0.9 (cf. Fig. 1B) indicating that canonical *ZFTA-RELA* fusions are present in a significant subset of ST-EPN that are molecularly distinct from classical ST-EPN-RELA based on DNA methylation profiling. Tumors from clusters 2 and 4 contained fusions to *ZFTA* but without involvement of *RELA*. Alternative *ZFTA* fusion partners included *MAML2* (n = 15), *MAML3* (n = 2), *NCOA1* (n = 2), *NCOA2 (*n = 9), and *CTNNA2* (n = 1) (Fig. 2A, B, C and Supplementary Table S1). Within remaining samples of the satellite clusters 2 and 4, no fusion (2/33) or fusions without involvement of *ZFTA* (2/33) were detected, respectively (Fig. 2A, Supplementary Table S1).

ZFTA-RELA fusions were identified in the majority of samples from the established ST-EPN-RELA group (63/70; 90.0%) (Supplementary Table S1). Within ST-EPN-RELA we observed a tendency of samples to cluster according to their respective fusion type (Supplementary Fig. S4A). Occasionally, analyses of samples from ST-EPN-RELA revealed more complex rearrangements including alternative fusions, such as *ZFTA-SS18* (n = 1/70), *SYVN1-MAJIN* (n = 1/70), and *RELA-MACROD1-ZFTA* (n = 1/70) (Supplementary Fig. S4B). In 18 cases belonging to ST-EPN-RELA (n = 14), cluster 1 (n = 3) and 3 (n = 1), more than one genetic fusion harboring either *RELA* or *ZFTA* was detected. However, all of these showed low confidence scores and may represent non-functional byproducts of structural rearrangements on chr. 11(6). For all samples from the satellite clusters (6/48) and for *ZFTA-RELA*-negative cases from the ST-EPN-RELA cluster (2/4) with sufficient material, alternative rearrangements were validated by RT-PCR followed by Sanger sequencing. In-frame fusion transcripts were confirmed in all cases (Supplementary Fig. S4C and Supplementary Table S1).

ST-EPN with alternative fusions show distinct transcription profiles and atypical histologies

To investigate whether (epi)genetically defined clusters of diagnostically ambiguous ST-EPNs also show transcriptional differences, we further analyzed available expression profiles (n = 66). Unsupervised hierarchical clustering analysis recapitulated clusters 1-4 derived from methylation data (Supplementary Fig. S5A). Exploration of differentially expressed genes (DEGs) and gene ontology (GO)-analysis comparing ST-EPN-RELA and clusters 2, 3, and 4 (FFPE-derived RNA-seq data were only available for n = 1 in cluster 1) revealed differences in expression patterns and activated signaling pathways (Supplementary Fig. S5B and C). *RELA* was significantly

upregulated in ST-EPN-RELA only. Previously described gene networks for ST-EPN-RELA, such as MAPK-signaling and synapse organization, were found predominantly active in this group (6). Cluster 2 showed upregulation of metabolic pathways, especially with regard to amino acid metabolism, while clusters 3 and 4 revealed activation of neuroendocrine signaling (Supplementary Fig. S5C). Integration with DEGs from a previously published dataset on signature genes in EPN and with (super-)enhancer-regulated genes in ST-EPN-RELA identified only very few shared DEGs with the new clusters but strong overlap with the ST-EPN-RELA group from this study (6,22) (Supplementary Fig. S5D-G). A substantial number of (super-)enhancers specific to ST-EPN-RELA were also associated with clusters 2 and 3, implying a shared set of genes regulated by *ZFTA*-associated fusion proteins in (Supplementary Fig. S5D-G, Supplementary Table S3).

Tumors harboring alternative rearrangements, or in case of cluster 3 also canonical *ZFTA-RELA* fusions, exhibited a broad spectrum of institutionally diagnosed high-grade and undifferentiated histologies including characteristics reminiscent of sarcoma, diffuse high-grade glioma, CNS embryonal tumors and other primitive tumors (Fig. 3A-E, Supplementary Fig. S6, S7A-J, S8A-F and Supplementary Table S4). In addition, a *ZFTA-RELA* fusion was detected in a case primarily diagnosed as centrally located malignant peripheral nerve sheath tumor as well as in a tumor that histologically appeared as ‘astroblastoma’. L1CAM, a characteristic histopathological marker for ST-EPN-RELA (23,24), and nuclear p65, the protein encoded by *RELA*, could be evaluated by immunohistochemistry (IHC) in a limited number of samples from cluster 2, 3 and 4 as well as in *ZFTA-RELA*-negative and *ZFTA-RELA* type 8 cases. Apart from one sample in cluster 2, all cases expressed L1CAM to different extents, demonstrating that L1CAM-expression is not restricted to tumors harboring canonical *ZFTA-RELA* fusions (Fig. 3F-I, Supplementary Table S4). IHC stainings for p65 were negative in cluster 2 (0/3) and in one sample from cluster 3 harboring a *ZFTA-RELA* fusion (1/4), and positive in cases across cluster 1 (n = 1), cluster 3 (n = 3), and cluster 4 (n = 1) (Fig. 3J-M, Supplementary Table S4). While *ZFTA-RELA* fusions were detected in 5/6 p65-positive cases, the p65-positive case from cluster 4 harbored a *ZFTA-CTNNA2* fusion, demonstrating that p65-positivity is not confined to *ZFTA-RELA* fusions. Upon central histopathological review of available tumors (n = 25), most cases were found to be at least compatible with variants of highly dedifferentiated ependymoma (Supplementary Table S4).

Collectively, these results suggest that *ZFTA* is an integrally promiscuous partner within potentially oncogenic fusion genes that drive transcriptionally distinct ST-EPN including cases with atypical histological characteristics.

A shared ZFTA DNA binding domain is essential for tumor formation *in vivo*

The *ZFTA-RELA* fusion gene has been shown to drive tumor formation, when delivered to neonatal mouse forebrain cells positive for either NESTIN, GFAP or BLBP using the RCAS/tv-a system (13), suggesting that ST-EPN-RELA formation may result from single-hit oncogenesis in cells at an early stage during development. This prompted us to test whether the respective fusions detected in clusters 1-4 are sufficient to cause tumor formation as well. To investigate this, recurrently identified fusion genes encoding *ZFTA* fused to *RELA*, *MAML2*, *MAML3*, and *NCOA2* were inserted into the pT2K-Luciferase-based expression vector flanked by *Tol2* cis elements. Genomic integration of the fusion genes into cells of the cortical ventricular zone was achieved by *in utero* electroporation-based transfection with co-expression of the Tol2 transposase (T2TP) at embryonic day 13.5 (E13.5) (Fig. 4A). According to our previous study (14), electroporation of *ZFTA-RELA* and *YAP1-MAMLD1* alone induced tumor formation within the cerebral cortex with a median survival of 44 days and 29.5 days (n = 11/11 for *ZFTA-RELA* and n = 30/30 for *YAP1-MAMLD1*), whereas no tumors were developed by overexpression of wildtype *ZFTA* (n = 0/13) (Fig. 4B). Overexpression of *ZFTA-MAML2* (n = 11/11), *ZFTA-MAML3* (n = 5/11) and *ZFTA-NCOA2* (n = 5/5) induced tumors with a median survival of 29, 103 and 36 days after birth, respectively (Fig. 4B). Histopathological analysis of mouse tumors displayed several common histological features among ZFTA fusion-driven tumors. All tumors presented with high density of monomorphous round to oval cells, similar to human EPN, and were similarly sharply demarcated from the surrounding brain (Fig. 4C-F). Thus, newly identified *ZFTA*-related fusion genes alone are sufficient to drive tumorigenesis *in vivo*.

Given that i) immunohistochemistry using an antibody against hemagglutinin (HA)-tagged fusion proteins revealed nuclear localization of the ZFTA-associated fusion proteins in all fusion-engineered tumors (Fig. 4G-J) and ii) the most N-terminal zinc finger DNA binding domain (ZF1) of ZFTA is shared by all fusion proteins (Fig. 2B), we hypothesized that this ZFTA DNA-binding domain is required for the oncogenic capacity of the fusions. In fact, *in utero* electroporation of *ZFTA* fusion genes lacking

the ZF1 coding region (ΔZF1) failed to develop tumors (Fig. 4K, L, Supplementary Fig. S9A and B). While ZFTA(ΔZF1)-RELA were not detected in the nucleus, nuclear localization capacity of ZFTA(ΔZF1)-MAML2 and ZFTA(ΔZF1)-NCOA2 proteins was still retained (Supplementary Fig. S9C-E), strongly suggesting other roles than nuclear shuttling of the shared ZF1 domain for tumorigenesis. Indeed, a co-submitted manuscript by Kupp et al. demonstrates that chromatin binding and recruitment of chromatin remodeling complexes is related to the single ZF1 domain in ZFTA-RELA (21).

Transactivation domains (TADs) represented another shared element among oncogenic fusion genes (Fig. 2B). To further investigate the role of TADs for tumor formation, ZFTA was fused to potent TADs, VP64 or EP300 (Supplementary Fig. S9F). None of the animals electroporated with ZFTA-VP64 or ZFTA-EP300 developed tumors during surveillance over 12 months (Supplementary Fig. S9G, n = 0/6). These findings suggest that additional oncogenic mechanisms are associated with the respective fusion partners. Importantly, this does not preclude an oncogenic role for the TAD within ZFTA-RELA and alternative fusion types, as Kupp et al. demonstrated that the TAD of RELA contributes to the fusion-associated transcriptional program through recruitment of transcriptional co-regulators (21).

Murine tumor models share molecular characteristics with human ST-EPN-RELA

For direct comparison of tumor models and human tumors, we applied principal component analysis to transcriptional profiles across species considering human and mouse orthologues. This approach revealed extensive molecular differences between *ZFTA* fusion- and *YAP1-MAMLD1*-driven tumors (Fig. 5A) (14). In order to control for species-specific effects and to provide variance measurements between murine models and human tumors, a hierarchical clustering was performed. This approach revealed high similarity between molecular groups of human ST-EPN and respective murine counterparts at the level of transcription (Fig. 5B). The strong effect on the transcriptome could also be demonstrated for another ZFTA-RELA-driven mouse model generated by Arabzade et al. (Supplementary Fig. S10A) (20). While others found global (Arabzade et al.) or focal (Kupp et al.) changes of histone marks (H3K27ac and H3K27me3) in murine tumor cells, we observed abundant global H3K27 trimethylation and acetylation in our ZFTA fusion-driven mouse models corresponding well to respective levels in human tumors (Supplementary Fig. S10B-R) (20,21).

Author Manuscript Published OnlineFirst on April 20, 2021; DOI: 10.1158/2159-8290.CD-20-0963
Author manuscripts have been peer reviewed and accepted for publication but have not yet been edited.

Since overexpression of *L1CAM* and activation of the NF-κB signaling pathway are molecular features of ST-EPN-RELA (7), we next examined these characteristics in *ZFTA* fusion-driven murine tumors. *Ccnd1* but not *L1cam* was highly expressed across all types of the fusion-driven tumors (Fig. 5C and D). However, a global activation of the NF-κB pathway was not observed in any model of the alternative fusion types, indicating that aberrant activity of this pathway is not contributing to tumorigenesis (Supplementary Fig. S11A and B). In line with these findings, Kupp et al. observed that altering the Rel-homology domain in ZFTA-RELA fusions, which represents the DNA binding domain shared by the NF-κB family proteins for their signal transduction, did not result in loss of oncogenicity (21).

Cross-species analysis identifies putative oncogenes downstream of ZFTA-fusions

Since the DNA binding domain of ZFTA is required for oncogenicity, we further explored common downstream effectors induced by transactivation of the *ZFTA*-associated fusion genes. To this end, we chose a cross-species approach to concisely match signaling pathways between human tumors and mouse models. To exclude transcriptional information governing ependymoma cell identity and programs across molecular groups that we had observed previously (22), we selected differentially expressed genes for human primary ST-EPN-RELAs significantly upregulated compared to all other molecular groups of EPNs (n = 3,825 genes) (Fig. 6A). A similar approach was used to compare gene expression data from *ZFTA*-driven mouse tumors against data from murine *YAP1-MAMLD1* tumors representing the only available alternative faithful model system (14). We found that 2,637 genes shared by ZFTA fusion-driven murine tumors are significantly higher expressed in comparison to *YAP1-MAMLD1* tumors (Fig. 6A). Filtering for orthologues in both mouse and human data resulted in 535 genes commonly upregulated in *ZFTA* fusion-related tumors across species (Fig. 6A). We next hypothesized that the list of these 535 genes includes the effector genes of characterized and uncharacterized oncogenic signaling commonly upregulated by *ZFTA* fusion genes. A gene ontology analysis revealed enrichment for cancer-related signaling pathways and partly convergence into known ST-EPN-RELA group-associated pathways, e.g., MAPK signaling (Supplementary Table S5) (6). We also found well-known oncogenes, such as the sonic hedgehog (Shh) mediator gene *GLI2*, the Wnt-mediator gene *LEF1* and the ependymoma oncogene *EPHB2* being

shared by ZFTA fusion-driven tumors (Fig. 6B) (3,25,26). All three genes were specifically upregulated in human ST-EPN-RELA as compared to other molecular groups of EPNs (Supplementary Fig. S12A-C). In addition, a comprehensive cross-species analysis by Kupp et al. comprising all mouse models deployed by the three independent co-submitted studies and the two largest published datasets of human ST-EPN-RELA identified a common fusion-associated signature of 93 genes that also included *GLI2* and *EPHB2* (6,7,20,21). To further explore potential direct interactions of *ZFTA* fusions with these genetic loci, we performed ChIP-seq with antibodies against HA and H3K27ac as well as ATAC-seq analyses on *ZFTA-RELA*-driven murine tumor cells (Supplementary Methods). Indeed, the *ZFTA-RELA* fusion was found to directly bind to H3K27ac-marked open chromatin regions of *Gli2*, *Lef1* and *Ephb2* (Fig. 6C-E). Consistent with our observation, the co-submitted study by Kupp et al. found that the ZFTA portion is capable of binding these loci (21). Reanalysis of ChIP-seq data on human tumors further supported these findings (Supplementary Fig. S12D-G).

GLI2 represents a candidate downstream gene in *ZFTA* fusion-driven tumorigenesis *in vivo*

To examine a potential functional implication of the revealed genes for *ZFTA*-driven tumorigenesis, we subsequently electroporated *ZFTA-RELA* together with genes encoding a dominant-negative form of GLI2, LEF1 and EPHB2, respectively (Fig. 7A). While the genes encoding the C-terminal portion of LEF1 (27) and the ectodomain of EPHB2 (28) did not attenuate tumor growth (Fig. 7B), the N-terminal portion of GLI2 (dnGLI2) that inhibits GLI2-mediated transactivation (29) prevented tumor formation (Fig. 7B and C), indicating the requirement of GLI2 function for *ZFTA* fusion-associated tumorigenesis. In line with this finding, GLI2 protein expression was elevated in human primary tumors harboring different types of *ZFTA* fusion genes as well as in corresponding murine tumor models (Supplementary Fig. S13A-H). Moreover, we found that *GLI2* transcription factor binding sites were highly enriched in histone H3K27ac-marked enhancers and super-enhancers of human ST-EPN-RELAs reported in our previous study (22) (Fig. 7D), further highlighting a decisive role of this oncogene.

To investigate the contribution of GLI2 to ST-EPN-RELA tumor progression, we next infected EP1NS, a *ZFTA-RELA*-expressing ST-EPN cell line, with dox-inducible shRNAs against *GLI2* (shGLI2_1 and shGLI2_2)- and non-targeting control shRNA

(shControl)-encoding lentiviruses. Approximately 40% reduction of *GLI2* transcripts were observed 48h after administration of doxycycline (2 µg/mL) (Fig. 7E). Within 96h after shRNA induction, EdU pulse-labeling revealed significant reduction of cell proliferation in GLI2 shRNA-expressing cells when compared to shControl (Fig. 7F). Annexin V staining also confirmed induction of enhanced apoptotic cell death in GLI2 shRNA-expressing cells (Fig. 7F). To further evaluate GLI2 inhibition *in vivo*, tumor bearing animals were treated with arsenic trioxide (ATO), a blood brain barrier-penetrating drug that includes GLI2 in its target spectrum (30-32). *ZFTA-RELA*-electroporated mice were treated with either 2.5 mg/kg ATO or vehicle (i.p. injection, 5 times per week) after the luciferase signal reached ca. $5x10^6$ photons/sec. ATO-treated animals showed extended survival when compared to vehicle-treated controls (Fig. 7G and Supplementary Fig. S13I). Comparable expression levels of *Gli2* were detected between control and ATO-exposed tumors (Supplementary Fig. S13J), thus excluding that ATO treatment incidentally downregulated *Gli2 in vivo*. Together, this data suggests GLI2 as potential therapeutic vulnerability in *ZFTA* fusion-positive tumors.

Discussion

In this study, we aimed to further investigate the biological heterogeneity of ST-EPN as a basis for future improved diagnostic accuracy and target identification. To this end, we performed a comprehensive molecular analysis of ST-EPN that confirmed previously described stable molecular groups of EPN but also identified additional satellite clusters related to ST-EPN-RELA. The *RELA* fusion partner *ZFTA* was found to be a recurrent partner in alternative translocations within tumors that constitute these satellite clusters. The clinical significance of these satellite clusters needs to be confirmed in future studies with increased sample size and clinical information. The clusters will be included in the upcoming version 12 of the Heidelberg Brain Tumor Methylation Classifier as part of a novel molecular family of *ZFTA*-fusion-related ST tumors.

Diagnostic assessment of cases within satellite clusters appears to be particularly challenging as tumors often not only harbor alternative *ZFTA* fusions but can also present histological characteristics untypical for ependymoma. While tumors in clusters 1 and 2 were predominantly diagnosed as ependymoma, other institutional

histological diagnoses were reported almost exclusively for clusters 3 and 4. Notably, immunohistochemical stainings for both L1CAM- and p65- could not reliably distinguish between *ZFTA*-RELA and other *ZFTA*-related fusions. Two previous case reports also described diagnostically ambiguous situations with a *ZFTA-RELA* fusion shared between a primary supratentorial ependymoma and its relapse, which histologically was diagnosed as sarcoma, and appearance of the fusion in an atypical teratoid/rhabdoid tumor (33,34). These findings further illustrate the diagnostic challenges imposed by these exceedingly rare tumors and indicate the potentially arbitrary role of histomorphology that does not necessarily reflect underlying molecular programs, as described for CNS-PNETs (35). These data further underpin the classification as planned for the upcoming 5th edition of the WHO Classification of Central Nervous System Tumours that allows for molecularly defined tumor types rather than adhering to strictly morphology-defined entities. We suggest that these oncogenic alterations may affect cells that had remained in an early stemness state permissive for one-hit tumorigenesis and rendering possible the development of morphologically non-neuronal, non-glial elements. This is supported by data in a co-submitted manuscript by Arabzade et al*.* identifying transcriptional programs within fusion-driven ependymoma that are active during embryonic brain development (20).

In the present study, we revealed the expression of various ZFTA fusion proteins in ST tumors. Each of these fusion proteins by itself caused tumor formation in the cerebral cortex, implying that they share oncogenic mechanisms. In line with Kupp et al*.* (21), we indeed identified a zinc finger DNA-binding domain of the fusion partner ZFTA as an essential element for tumorigenesis, which also resulted in the new official designation of the gene formerly known as *C11orf95*. In addition, structural comparison of all ZFTA fusion partners identified the common presence of a transactivation domain, raising the possibility that ZFTA fusion oncoproteins activate oncogenes through recruitment of an activating domain to the ZFTA bound targets. Notably, each of the newly identified *ZFTA* fusion genes induced tumors with different penetrance and latency. This may be attributed to variable effects of the fusion partners on the transcriptional machinery in neural progenitors. For instance, MAML2 and MAML3 have been known to be a cofactor of NOTCH, which is responsible for clonal expansion of cortical progenitors in the ventricular zone. However, MAML2 shows much stronger transcriptional activation of *Hes* genes than MAML3 (36). Therefore, *ZFTA-MAML2*-mediated enhancement of NOTCH signaling is likely to increase the number of fusion

bearing progenitors more efficiently. Consistent with this idea, we indeed found reduced survival in mice electroporated with *ZFTA-MAML2* compared to *ZFTA-MAML3* (Fig. 4B). Considering that NF-κB signaling is involved in neural stem cell (NSC) proliferation in the cerebral cortex (37,38), *ZFTA-RELA* is also likely to expand the progenitor pool of the transfected cells, thus shortening the latency of tumor formation. Since ST tumors associated with different fusions are characterized by variable methylation profiles, it could also be hypothesized that each fusion oncoprotein may exert transformation activity in distinct NSC subtypes already committed to specific progenitors, as was reported for medulloblastoma (39,40). Notably, applying single cell RNA-sequencing to a cohort of ST-EPN-RELA and posterior fossa group A ependymoma (PF-EPN-A) we and others previously recognized a larger inter-tumoral heterogeneity for *ZFTA-RELA*-driven tumors compared with PF-EPN-A (41). Future single cell studies coupled with technologies for profiling the chromatin landscape may enable the inference of developmental lineages.

A previous animal study revealed the NF-κB- and non-NF-κB-related impact of *ZFTA-RELA* fusions on tumor formation by mutagenesis (13). A mutation of the Rel-homology domain failed to drive tumorigenesis, whereas alterations of the transactivation domain still resulted in tumor formation. In our study, we did not observe NF-κB pathway activation in tumors without *RELA* as fusion partner. In keeping with this notion, Arabzade et al. demonstrated that a major component of the fusion binding is tumor-specific and not observed in canonical NF-κB-related gene expression (20). In addition, Kupp et al. found that the Rel-homology domain is not required for fusion-driven gene expression (21). It remains to be further elucidated if at least transactivation domains that represent a shared pattern between fusions that cluster together and lack the Rel-homology domain, such as *ZFTA-NCOA1*, *ZFTA-NCOA2* and *ZFTA-MAML2*, may contribute to tumorigenesis through binding of transcriptional cofactors. Indeed, integrated cross-species analyses identified downstream targets shared by ST tumors with *ZFTA* fusions suggesting similar transcriptional activation processes. Our results stress that *GLI2* functions as a relevant downstream oncogene in *ZFTA* fusion-driven ST tumors and pharmacological inhibition could significantly reduce tumor growth.

In summary, we demonstrate the transforming capacity of *ZFTA*-containing fusions, provide representative mouse models, and present a rationale for further preclinical studies blocking central molecular dependencies of these fusions. Tumors

containing a canonical or alternative *ZFTA* fusion will be classified as supratentorial ependymoma, *ZFTA* fusion-positive in the upcoming 5th edition of the WHO Classification of Central Nervous System Tumours.

Methods

Animals

CD-1 mice used for *in utero* electroporation were obtained from Charles River and housed in a vivarium with a 12h light/dark cycle with access to food and water ad libitum. The day of the plug and the birthdate are designated as embryonic day (E) 0.5 and postnatal day (P) 0, respectively. All animal experiments for this study were conducted according to the animal welfare regulations approved by the Animal Care and Use Committee of the National Institute of Neuroscience, NCNP in Japan (Approval number: 2019028R1) and the responsible authorities in Germany (Regierungspräsidium Karlsruhe, approval number: G-255/19 and G-260/19).

Human Subjects

All experiments in this study involving human tissue or data were conducted in accordance with the Declaration of Helsinki. Tumor material (Fresh Frozen Paraffin-embedded (FFPE) tissue, pre-isolated RNA and/or DNA) or information on molecular tumor characteristics was collected and analyzed after receiving written informed consent from the respective patients or their legal representatives and according to the guidelines of the ethical institutional review boards of the participating institutions, such as Heidelberg University Hospital and the NN Burdenko Neurosurgical Institute. For cases from diagnostic or clinical studies, material was obtained in accordance with the respective study protocol and informed consents. For all cases, a genotype check was performed to exclude the possibility that material from the same patient was received from more than one center. To this end, the Pearson correlation across beta methylation values of 59 rs-loci present on both the Illumina Infinium HumanMethylation450 and the Illumina Infinium HumanMethylation EPIC array were calculated. Samples with a correlation ≥ 0.95 were considered as genotype matches.

Cell Line

HEK-293T (CRL-3216) cells were purchased from ATCC. HEK-293T cells were cultivated with Dulbecco's Modified Eagle Media (DMEM, Thermo Fisher) supplemented with heat-inactivated 10% fetal bovine serum (FBS, Thermo Fisher), 2 mM L-glutamine, 100 U/mL penicillin and 100 µg/mL streptomycin. The cells were maintained in a humidified 5% CO_2 atmosphere at 37 °C and subcultured when cell confluency reached approximately 80%. Mycoplasma contamination was assessed periodically by GATC/Eurofins.

Plasmids cloning

The full or partial coding regions of human *ZFTA*, *MAML2, MAML3* and *NCOA2* cDNAs with a C-terminal HA tag were amplified by PCR and cloned into pT2K-IRES-Luc plasmid vectors using In-Fusion HD Cloning kit (Takara Bio). Dominant negative *Gli2* was amplified by RT-PCR on total RNA of mouse granular neural progenitor cells. pT2K plasmids were co-transfected with Tol2 transposase encoded in the pCAGGS plasmid. For the generation of *ZFTAΔZF1-RELA/MAML2/NCOA2* cDNA, a sequence of zinc finger domain was chosen based on UniProt prediction. All primers used for PCR are listed in Supplementary Table S6.

Generation of Dox-inducible shRNA-expressing cells.

Human EPN cell line EP1NS was transduced with lentiviral pLKO-tet-on vector system (plasmid #21915, Addgene) containing a puromycin-resistance gene, and a tet-responsive element for dox-inducible expression of shRNA against GLI2 (shGLI2_1 and shGLI2_2) or a non-targeting control shRNA (shControl). All primers used for cloning are listed in Supplementary Table S6. The dox-inducible vectors were generated according to a publicly available protocol (42,43). Lentiviral particles were generated in HEK293T cells. Virus-containing supernatant was collected to infect EP1NS cell line. Infected cells were selected with 1 µg/mL puromycin. The shRNA expression for *GLI2* knockdown in EP1NS was achieved by adding 1 µg/mL doxycycline every 48h to the medium. For proliferation assay, 96h after dox administration, the cells were treated with EdU (final concentration: 10 µM) for 12h and subsequently harvested with Accutase solution. EdU-incorporated cells were labeled using a Click-iT EdU Alexa Fluor 647 Flow Cytometry Assay Kit (Life Technologies) according to the manufacturer's protocol. The cells were passed through a 35 µm cell

strainer yielding a single cell suspension and analyzed by flow cytometry using a FACS Fortessa flow cytometer (BD Biosciences). For apoptosis assay, the infected cells were harvested 96h after dox treatment, and were subsequently washed twice with Cell Staining Buffer (BioLegend). Cells were then stained with Annexin V-APC and DAPI diluted in Annexin V Binding Buffer using Apoptosis Detection Kits (BioLegend) according to the manufacturer's protocol. Samples were analyzed by flow cytometry using a FACS Fortessa flow cytometer (BD Biosciences).

In utero electroporation

In utero electroporation was performed as reported previously (44). Specifically, endotoxin-free DNA plasmid mixture (1 μg/μL for each plasmid) were injected into the lateral ventricle of E13.5 embryos, and square electric pulses (32 V, 50 ms-on, 450 ms-off, five pulses) were delivered using 5 mm-diameter platinum forceps-like electrodes (BTX). For *in vivo* tumor formation analysis, electroporated animals were selected at neonatal stages by intraperitoneal (i.p.) injection of D-Luciferin (150 mg/kg) and subsequent bioluminescence imaging. Growth of transfected cells was monitored every week by measurement of intensity of bioluminescence with IVIS Lumina LT Series III Caliper (Perkin Elmer). The animals were sacrificed, once they exhibited neurological signs, such as head tilting, abnormal gait, and a hunched posture, or at 1 year of age if showing no symptoms.

In vivo ATO treatment

A stock solution of 20 mg/mL ATO in 1 M NaOH was prepared. It was further diluted to 0.5 mg/mL ATO with PBS, and the solution was sterile-filtrated. The vehicle solution was prepared the same way but without ATO. When the bioluminescence signal of the electroporated animals reached ca. 5 x 10^6 photo/second, the animals were allocated randomly to vehicle- and ATO-treatment group and treated five days per week either with 2.5 mg ATO/kg/day (i.p). or the equivalent volume of vehicle solution. Prior to the treatment, 20% mannitol in 0.9% saline was i.p injected into mice (5 mL/kg) to disrupt the blood–brain barrier. The mice were monitored daily for tumor-specific symptoms and euthanized when it exhibited neurological symptoms.

Immunohistochemistry staining

Brains with tumor from electroporated mice were dissected and fixed with formalin at

4 °C for 48h. 5 μm-thick paraffin-embedded murine tumor sections were immunostained according to the procedures in our previous study (45). After deparaffinization, the sections were pre-treated with citrate buffer at 100 ˚C for 30 minutes. Then the sections were incubated with the primary antibodies (Supplementary Table S7) diluted with Dako REAL Antibody Diluent (Agilent #S2022) at room temperature (RT) overnight. DAB staining was performed the next day using SuperVision 2 HRP-polymer kit (DCS PD000POL) following the protocol provided by the manufacturer. Slides were mounted in ProLong Gold Antifade Mountant (Invitrogen #P36930). Nuclei were stained with DAPI (300 nM). Images were acquired with confocal microscopes (ZEISS Cell Observer).

Immunohistochemistry for human samples was performed on a Ventana BenchMark ULTRA Immunostainer (Ventana Medical Systems, Tucson, AZ, USA). Antibodies used in this study are listed in Supplementary Table S7.

Immunofluorescence staining

HEK293T cells were cultured on glass coverslips one day before transfection. Plasmid constructs were transfected using Fugene (Promega) following the instructions provided by manufacturer. 48h after transfection, cells were fixed with 4% paraformaldehyde for 20 minutes followed by 10 minutes permeabilization with Triton buffer (0.1% Triton in PBS). After washing with PBS two times, the primary antibody (Supplementary Table S7) was applied directly on the cells for 1 hour at RT. The antibody solution was removed by absorption with Whatman filter paper before washing the coverslips two times 5 minutes with PBS. The corresponding secondary antibody was applied subsequently, incubated for 30 minutes and three times washed for 5 minutes in PBS. Finally, cells were washed briefly in ddH_2O in order to remove salts and pure ethanol before they were mounted on microscopy glass slides with Fluoromount-G^{TM} containing 1 μg/mL DAPI (Southern biotech).

Western blotting

The protein expression of the plasmids used in this study was validated by western blotting according to the following procedures: HEK293T cells were transfected with the plasmids and harvested 48h after transfection. The cell pellets were lysed with RIPA buffer and 20 μg of the protein lysates were used for protein detection. Briefly, proteins were denatured for 5 minutes at 95 °C, loaded on NuPAGE Bis-Tris

(#NP0301BOX, Invitrogen) and separated at 120 V for 2h. Proteins were transferred to methanol-activated PVDF membrane by tank electrotransfer in Towbin buffer for 1h at 110 V. Membrane was blocked with 5% skimmed milk in 0.5% Tween/TBS (TBST) for 1h at RT prior to overnight incubation with primary antibodies (Supplementary Table S7). After washing with TBST, membrane was incubated with secondary antibody for 1h at RT. The membrane was developed with either ECL (RPN2106, GE Lifesciences) or ECL Prime (RPN2232, GE Lifesciences) as recommended by the manufacturer followed by exposure to autoradiography films in a dark room.

As for H3K27me3 and H3K27ac analysis, mouse brains were lysed in Lysis buffer (150 mM NaCl, 20 mM Tris-HCl (pH 7.4), 2 mM EDTA, 1% NP-40) and sonicated with a Bioruptor. The lysates were collected after centrifugation (13,000 × g for 10 minutes) and then denatured in SDS sample buffer at 95 °C for 3 minutes. 0.1 μg and 10 μg of the lysates were used for Histone H3 and for H3K27ac and H3K27me3, respectively. Blotted membranes were blocked with 5% non-fat milk in TBST for 30 minutes and immunoblotted with anti-Histone H3 (Abcam, ab1791, 1:1000), anti-Tri-methyl-Histone H3 (K27) (Abcam, ab6002, 1:300) and anti-Acetyl-Histone H3 (K27) (CST, D5E4, 1:300) antibodies. After washing, the membranes were incubated with HRP-conjugated secondary antibodies (GE Healthcare, 1:1000) for 1h at room temperature. Then they were washed at least four times and detected via enzyme-linked chemiluminescence (Immobilon Forte; Millipore) in a cooled CCD camera (LAS-4000 mini, Fujifilm). For quantitative analysis, the signal intensities from murine tumor lysates were measured with the image J software and normalized by a global level of histone H3.

RNA Isolation

Total RNA was extracted from cryo-preserved mouse tissues using an RNeasy Plus Mini Kit together with QIAshredder (QIAGEN) according to manufacturer's instructions and stored in -80 ºC until use. cDNAs for downstream application were prepared using the SuperScript VILO cDNA Synthesis Kit (Invitrogen).

Quantitative RT-PCR

qPCR mix was prepared following manufacturing protocol of Power SYBR Green PCR Master Mix (Applied Biosystems). qPCR was performed using the QuantStudio 5 RT-PCR system (Applied Biosystems). The cycling conditions used were 95 °C for 10

minutes and 40 cycles of 95 °C for 15s and 60 °C for 1 minutes following dissociation analysis. All qPCR reactions were done in triplicate and normalized to TBP mRNA levels.

DNA-methylation profiling and Copy Number Variation Plots (CNVs)

Genome-wide DNA methylation profiling was performed using the Illumina Infinium HumanMethylation450 and the Illumina Infinium HumanMethylation EPIC Kits as previously described and according to the manufacturer's instructions (6).

All computational analyses were performed in R version 3.4.4 (R Development Core Team, 2019). Raw signal intensities were obtained from IDAT-files using the minfi Bioconductor package version 1.24.0 (46,47). Illumina EPIC and 450k samples were merged to a combined data set by selecting the intersection of probes present on both arrays (combineArrays function, minfi). Each sample was individually normalized as described in (14). Subsequently, a correction for the type of material tissue (FFPE/frozen) and array (450k/EPIC) was performed by fitting univariate, linear models to the log2-transformed intensity values (removeBatchEffect function, limma package version 3.34.5). The methylated and unmethylated signals were corrected individually before beta-values were calculated. CpG probes selection was performed as described in (14). In total, 428,230 probes were kept for downstream analysis.

To perform unsupervised non-linear dimension reduction, the remaining probes were used to calculate the 1-variance weighted Pearson correlation between samples by applying the function wtd.cors function of the R-package weights version 1.0.1. The resulting distance matrix was used as input for t-Distributed Stochastic Neighbor Embedding analysis (t-SNE; *Rtsne* package version 0.13). The following non-default parameters were applied: theta = 0, pca = F, max_iter = 2500 perplexity = 20.

In order to identify fitting samples for this study, an exploratory set of 20 cases was chosen on the basis of the following three conditions: i) prediction for ST-EPN-RELA according to DNA methylation-based classification but without evidence for a canonical *ZFTA-RELA* fusion, ii) the *vice versa* combination with a typical fusion event in the absence of a reliable ST-EPN-RELA score or iii) supratentorial tumors histologically diagnosed as EPN that cannot readily be assigned to any of the existing molecular classes. DNA-methylation profiles of these cases were clustered with a cohort of 61,821 samples from different tumor entities and experimental data and compared with a reference set (15). This analysis was subsequently repeated with an

increased set of 71,270 samples and with a reference cohort of 507 EPN cases covering all 10 major subgroups (5,6).

The 613 samples in the cohort were assigned to either ST-EPN-RELA, satellite cluster 1 - 4 or outlier cases based on a hierarchical density-based scan (HDBSCAN, R-package *dbscan* version 1.1-5 (48)) using the 2-dimensional projection resulting from the tSNE as input and applying a minPts parameter of 5. Cluster stability was assessed by a resampling approach. For each of 500 resampling iterations, tSNE dimension reduction followed by HDBSCAN cluster assignment was applied to 80% of the samples sampled without replacement. In accordance to Consensus Clustering (49), a consensus matrix was calculated storing pairwise relative frequencies how often two samples were assigned to the same cluster. A heatmap of the consensus matrix was generated applying the pheatmap R-package using the default settings for clustering rows and columns (Supplementary Fig. S2C). The heatmap was annotated with the HDBSCAN results for the complete data set as well with the frequency how often a sample was assigned to the outlier cluster over the resampling iterations. The distribution of the number of clusters detected over the 500 iterations is shown in Supplementary Fig. S2B indicating 6 as the most frequently identified number of clusters (ST-EPN-RELA, cluster 1 – 4, and outliers).

CNV analysis from 450k and EPIC methylation array data was performed using the conumee Bioconductor package version 1.12.0 (Hovestadt V, Zapatka M, 2017). Summary copy number profiles were created by summarizing these data in the respective sets of cases.

DNA-panel sequencing

DNA-panel sequencing was performed on 29 samples obtained from either FF- or FFPE-material using a customized enrichment/hybrid-capture-based next-generation sequencing (NGS) gene panel 130 genes recurrently altered in brain tumors according to the manufacturer's instructions and as previously described (50).

RNA-sequencing analysis and fusion discovery

High-throughput sequencing of 66 samples obtained from FFPE-material and 28 samples obtained from FF-material with sufficient quality and quantity of RNA was performed according to the manufacturer's instruction and as previously described

(5,51). General FFPE RNA-seq data processing (reads alignment, quality control and gene expression counts computation) was performed as previously described (51). Unsupervised analysis of tumor samples was performed with principal component analysis, tSNE and hierarchical clustering based on the selection of the top 1000 most variable genes with log2 RPKM normalized gene expression counts. Selection of the NF- κB target genes was derived from the corresponding source (https://bioinfo.lifl.fr/NF-KB/).

Fusion genes discovery from RNA-sequencing data was performed using two independent tools: InFusion (52) and Arriba (https://github.com/suhrig/arriba/). Transcription of fusion identified by RNA-sequencing was confirmed by RT-PCR. RNA was extracted from frozen tumor samples, then reverse-transcription and PCR were carried out by using OneStep RT-PCR Kit (QIAGEN), using specific primers (Supplementary Table S6). Fusions were confirmed by Sanger sequencing (Eurofins Genomics).

Tumor cross-species verification

The Affymetrix data cohorts were used for cross-species analysis. Human Affymterix data from corresponding study (6) was integrated from R2 system. The list of common mice-human gene orthologs from AGDEX Affymetrix reference (14635 genes in total) was integrated for gene probes selection in further comparison between human tumor and mouse model datasets. Initially differentially expressed orthologous genes between the ST-EPN-YAP1 and ST-EPN-RELA tumors starting from top 5000 most evident (min adjusted p-val < 0.0006) were applied as the target reference to confirm the model's correspondence based on unsupervised hierarchical clustering and principal component analysis as it was described previously (14). Further, in order to increase the specificity for ZFTA-driven effects, evident differentially expressed genes of ST-EPN-RELA tumors vs all other EPN subgroups were integrated for target candidate selection (n=3825, min. adjusted p-val < 0.05). Differentially expressed genes between models were detected using limma R package (53) with adjusted p-val < 0.05.

For the gene ontology and pathway analysis the common orthologs between mouse models and human tumors were selected from differentially expressed genes specific for ST-EPN-RELA against all other EPN subgroups and for each ZFTA-driven

model against MAMLD1-YAP1 control. Gene ontology analysis was performed using ClueGO tool (54) by focusing the top 300 top evident genes.

Statistical Analysis

The Kaplan-Meier-method was applied for survival analysis comparing the different fusion constructs and visualized using R version 3.6.1 (R Core Team, 2020) and the survival- and survminer-R packages (https://github.com/therneau/survival, https://github.com/kassambara/survminer). The Paired t test was used for EdU and Annexin V analysis in the shGLI2 experiment and visualized using GraphPad Prism.

Data and Code Availability

Data from methylation profiling, RNA-sequencing and DNA panel-sequencing will be deposited at the European Genome-phenome archive (https://www.ebi.ac.uk/ega/home).

Author's Contributions

Concept and design: T. Zheng, D.R. Ghasemi, K. Okonechnikov, A. Korshunov, M. Sill, K.K. Maass, D.T.W. Jones, S.M. Pfister, D. Kawauchi, K.W. Pajtler

Development of methodology: T. Zheng, D.R. Ghasemi, K. Okonechnikov, A. Korshunov, M. Sill, P. Benites Goncalves da Silva, S. Taya, T. Adachi, R. Shiraishi.

Acquisition of data (provided animals, acquired and managed patients, provided facilities, etc.): T. Zheng, D.R. Ghasemi, K. Okonechnikov, A. Korshunov, M. Sill, K.K. Maass, M. Hoshino, D.T.W. Jones, S.M. Pfister, A. von Deimling, F. Sahm, D. Kawauchi, K.W. Pajtler

Analysis and interpretation of data (e.g., statistical analysis, biostatistics, computational analysis): T. Zheng, D.R. Ghasemi, K. Okonechnikov, D. Stichel, A. Arabzade, R. Kupp

Writing, review, and/or revision of the manuscript: T. Zheng, D.R. Ghasemi, K. Okonechnikov, M. Kool, D.T.W. Jones, S.M. Pfister, F. Sahm, D. Kawauchi, K.W. Pajtler

Administrative, technical, or material support (i.e., reporting or organizing data, constructing databases): T. Zheng, D.R. Ghasemi, K. Okonechnikov, A. Korshunov, M. Sill, K.K. Maass, M. Ryzhova, J. Gojo, J. Benzel, N. U. Gerber, D. Sturm, J. Ecker,

F. Selt, R. Chapman, C. Haberler, A. Arabzade,D. Figarella-Branger, G. Reifenberger, G. Fleischhack, S. Rutkowski, A.M. Donson, V. Ramaswamy, D. Capper, D.W. Ellison, C. Herold-Mende, U. Schüller, S. Brandner, P. Hernáiz Driever, J.M. Kros, M. Snuderl, T. Milde, R.G. Grundy, M. Hoshino, S.C. Mack, R.J. Gilbertson

Study supervision: F. Sahm, D. Kawauchi, K.W. Pajtler

Acknowledgments

We thank the High Throughput Sequencing Unit of the Genomics & Proteomics Core Facility, German Cancer Research Center (DKFZ) for providing excellent services regarding all sequencing experiments. We are grateful to Norman Mack, Laura Sieber, Britta Statz, Monika Mauermann, Lukas Schmitt and Tatjana Wedig, Department of Pediatric Neurooncology, German Cancer Research Center, Laura Doerner, Lisa Kreinbihl, Jochen Meyer, Lea Hofmann and Moritz Schalles, Department of Neuropathology, Heidelberg University Hospital, for excellent technical assistance. This study was generously supported by the Ein Kiwi gegen Krebs-foundation. We thank the German Childhood Cancer Foundation for funding ("Molecular Neuropathology 2.0 - Increasing diagnostic accuracy in paediatric neurooncology" (DKS 2015.01)). Furthermore, this work was supported by fellowships of German Academic Exchange Service (DAAD) (T.Z.), the Mildred-Scheel doctoral program of the German Cancer Aid (D.R.G.), the German Academic Scholarship Foundation (D.R.G.), the Hertie Network of Excellence in Clinical Neuroscience (P.S.), the Else Kröner Excellence Program of the Else Kröner-Fresenius Stiftung (EKFS) (F.S.), a grant from the Japan Agency for Medical Research and Development, AMED (JP20ck0106534h0001), Fund for the Promotion of Joint International Research (19K24687, JSPS) (D.K.) and the Collaborative Ependymoma Research Network (CERN) fellowship (K.W.P.). U.S. was supported by the Gert und Susanna Mayer Stiftung and the Fördergemeinschaft Kinderkrebszentrum Hamburg. Part of the study was funded by the National Institute for Health Research to UCLH Biomedical research centre (BRC399/NS/RB/101410). S.B. was also supported by the Department of Health's NIHR Biomedical Research Centre's funding scheme. A.K. is supported by the Helmholtz Association Research Grant (Germany). M.R. is supported by the RSF Research Grant №18-45-06012. The methylation profiling at NYU is in part supported by the Friedberg Charitable Foundation and the Making Headway Foundation grants

(M.S.). We thank Maximilian Harkotte, Department of Psychology, Eberhard Karls University Tübingen, for advice regarding data analysis and Niklas Freund, MRC Laboratory of Molecular Biology and Cambridge University, for fruitful discussions. We are grateful to all patients and their families for taking part in this study.

References

1. Ostrom QT, Cioffi G, Gittleman H, Patil N, Waite K, Kruchko C*, et al.* CBTRUS Statistical Report: Primary Brain and Other Central Nervous System Tumors Diagnosed in the United States in 2012-2016. Neuro Oncol **2019**;21(Suppl 5):v1-v100 doi 10.1093/neuonc/noz150.
2. Ellison DW, Kocak M, Figarella-Branger D, Felice G, Catherine G, Pietsch T*, et al.* Histopathological grading of pediatric ependymoma: reproducibility and clinical relevance in European trial cohorts. J Negat Results Biomed **2011**;10:7 doi 10.1186/1477-5751-10-7.
3. Johnson RA, Wright KD, Poppleton H, Mohankumar KM, Finkelstein D, Pounds SB*, et al.* Cross-species genomics matches driver mutations and cell compartments to model ependymoma. Nature **2010**;466(7306):632-6 doi 10.1038/nature09173.
4. Mack SC, Witt H, Piro RM, Gu L, Zuyderduyn S, Stutz AM*, et al.* Epigenomic alterations define lethal CIMP-positive ependymomas of infancy. Nature **2014**;506(7489):445-50 doi 10.1038/nature13108.
5. Ghasemi DR, Sill M, Okonechnikov K, Korshunov A, Yip S, Schutz PW*, et al.* MYCN amplification drives an aggressive form of spinal ependymoma. Acta Neuropathol **2019**;138(6):1075-89 doi 10.1007/s00401-019-02056-2.
6. Pajtler KW, Witt H, Sill M, Jones DT, Hovestadt V, Kratochwil F*, et al.* Molecular Classification of Ependymal Tumors across All CNS Compartments, Histopathological Grades, and Age Groups. Cancer Cell **2015**;27(5):728-43 doi 10.1016/j.ccell.2015.04.002.
7. Parker M, Mohankumar KM, Punchihewa C, Weinlich R, Dalton JD, Li Y*, et al.* C11orf95-RELA fusions drive oncogenic NF-kappaB signalling in ependymoma. Nature **2014**;506(7489):451-5 doi 10.1038/nature13109.
8. Taylor MD, Poppleton H, Fuller C, Su X, Liu Y, Jensen P*, et al.* Radial glia cells are candidate stem cells of ependymoma. Cancer Cell **2005**;8(4):323-35 doi 10.1016/j.ccr.2005.09.001.
9. Witt H, Mack SC, Ryzhova M, Bender S, Sill M, Isserlin R*, et al.* Delineation of two clinically and molecularly distinct subgroups of posterior fossa ependymoma. Cancer Cell **2011**;20(2):143-57 doi 10.1016/j.ccr.2011.07.007.
10. Bouffet E, Foreman N. Chemotherapy for intracranial ependymomas. Childs Nerv Syst **1999**;15(10):563-70 doi 10.1007/s003810050544.
11. Merchant TE, Li C, Xiong X, Kun LE, Boop FA, Sanford RA. Conformal radiotherapy after surgery for paediatric ependymoma: a prospective study. Lancet Oncol **2009**;10(3):258-66 doi 10.1016/s1470-2045(08)70342-5.
12. Malgulwar PB, Nambirajan A, Pathak P, Faruq M, Rajeshwari M, Singh M*, et al.* C11orf95-RELA fusions and upregulated NF-KB signalling characterise a subset of

aggressive supratentorial ependymomas that express L1CAM and nestin. J Neurooncol **2018**;138(1):29-39 doi 10.1007/s11060-018-2767-y.

13. Ozawa T, Arora S, Szulzewsky F, Juric-Sekhar G, Miyajima Y, Bolouri H*, et al.* A De Novo Mouse Model of C11orf95-RELA Fusion-Driven Ependymoma Identifies Driver Functions in Addition to NF-kappaB. Cell Rep **2018**;23(13):3787-97 doi 10.1016/j.celrep.2018.04.099.
14. Pajtler KW, Wei Y, Okonechnikov K, Silva PBG, Vouri M, Zhang L*, et al.* YAP1 subgroup supratentorial ependymoma requires TEAD and nuclear factor I-mediated transcriptional programmes for tumorigenesis. Nat Commun **2019**;10(1):3914 doi 10.1038/s41467-019-11884-5.
15. Capper D, Jones DTW, Sill M, Hovestadt V, Schrimpf D, Sturm D*, et al.* DNA methylation-based classification of central nervous system tumours. Nature **2018**;555(7697):469-74 doi 10.1038/nature26000.
16. Fukuoka K, Kanemura Y, Shofuda T, Fukushima S, Yamashita S, Narushima D*, et al.* Significance of molecular classification of ependymomas: C11orf95-RELA fusion-negative supratentorial ependymomas are a heterogeneous group of tumors. Acta Neuropathol Commun **2018**;6(1):134 doi 10.1186/s40478-018-0630-1.
17. Pages M, Pajtler KW, Puget S, Castel D, Boddaert N, Tauziede-Espariat A*, et al.* Diagnostics of pediatric supratentorial RELA ependymomas: integration of information from histopathology, genetics, DNA methylation and imaging. Brain Pathol **2019**;29(3):325-35 doi 10.1111/bpa.12664.
18. Nowak J, Junger ST, Huflage H, Seidel C, Hohm A, Vandergrift LA*, et al.* MRI Phenotype of RELA-fused Pediatric Supratentorial Ependymoma. Clin Neuroradiol **2019**;29(4):595-604 doi 10.1007/s00062-018-0704-2.
19. Lillard JC, Venable GT, Khan NR, Tatevossian RG, Dalton J, Vaughn BN*, et al.* Pediatric Supratentorial Ependymoma: Surgical, Clinical, and Molecular Analysis. Neurosurgery **2019**;85(1):41-9 doi 10.1093/neuros/nyy239.
20. Arabzade A, Zhao Y, Varadharajan S, Chen HC, Jessa S, Rivas B*, et al.* ZFTA-RELA Dictates Oncogenic Transcriptional Programs to Drive Aggressive Supratentorial Ependymoma. Cancer Discov **2021** doi 10.1158/2159-8290.Cd-20-1066.
21. Kupp R, Ruff L, Terranova S, Nathan E, Ballereau S, Stark R*, et al.* ZFTA-translocations constitute ependymoma chromatin remodeling and transcription factors. Cancer Discov **2021** doi 10.1158/2159-8290.Cd-20-1052.
22. Mack SC, Pajtler KW, Chavez L, Okonechnikov K, Bertrand KC, Wang X*, et al.* Therapeutic targeting of ependymoma as informed by oncogenic enhancer profiling. Nature **2018**;553(7686):101-5 doi 10.1038/nature25169.
23. Wani K, Armstrong TS, Jones DT, Vera-Bolanos E, Witt H, Capper D*, et al.* BI-30: CHARACTERIZATION OF L1CAM AS A CLINICAL MARKER FOR THE C11orf95-RELA FUSION IN SUPRATENTORIAL EPENDYMOMAS. Neuro-Oncology **2014**;16(Suppl 5):v30-v doi 10.1093/neuonc/nou239.30.
24. Chavali P, Rao S, Palavalasa S, Bevinahalli N, Muthane YTC, Sadashiva N*, et al.* L1CAM Immunopositivity in Anaplastic Supratentorial Ependymomas: Correlation With Clinical and Histological Parameters. Int J Surg Pathol **2019**;27(3):251-8 doi 10.1177/1066896918800812.
25. Ruiz i Altaba A. Gli proteins and Hedgehog signaling: development and cancer. Trends in Genetics **1999**;15(10):418-25 doi https://doi.org/10.1016/S0168-9525(99)01840-5.
26. Nusse R. A Versatile Transcriptional Effector of Wingless Signaling. Cell **1997**;89(3):321-3 doi https://doi.org/10.1016/S0092-8674(00)80210-X.

27. Behrens J, von Kries JP, Kuhl M, Bruhn L, Wedlich D, Grosschedl R*, et al.* Functional interaction of beta-catenin with the transcription factor LEF-1. Nature **1996**;382(6592):638-42 doi 10.1038/382638a0.
28. Henkemeyer M, Orioli D, Henderson JT, Saxton TM, Roder J, Pawson T*, et al.* Nuk controls pathfinding of commissural axons in the mammalian central nervous system. Cell **1996**;86(1):35-46 doi 10.1016/s0092-8674(00)80075-6.
29. Takanaga H, Tsuchida-Straeten N, Nishide K, Watanabe A, Aburatani H, Kondo T. Gli2 is a novel regulator of sox2 expression in telencephalic neuroepithelial cells. Stem Cells **2009**;27(1):165-74 doi 10.1634/stemcells.2008-0580.
30. Shahi MH, Holt R, Rebhun RB. Blocking signaling at the level of GLI regulates downstream gene expression and inhibits proliferation of canine osteosarcoma cells. PLoS One **2014**;9(5):e96593 doi 10.1371/journal.pone.0096593.
31. Beauchamp EM, Ringer L, Bulut G, Sajwan KP, Hall MD, Lee YC*, et al.* Arsenic trioxide inhibits human cancer cell growth and tumor development in mice by blocking Hedgehog/GLI pathway. J Clin Invest **2011**;121(1):148-60 doi 10.1172/JCI42874.
32. Neumann JE, Wefers AK, Lambo S, Bianchi E, Bockstaller M, Dorostkar MM*, et al.* A mouse model for embryonal tumors with multilayered rosettes uncovers the therapeutic potential of Sonic-hedgehog inhibitors. Nature medicine **2017**;23(10):1191-202 doi 10.1038/nm.4402.
33. Nobusawa S, Hirato J, Sugai T, Okura N, Yamazaki T, Yamada S*, et al.* Atypical Teratoid/Rhabdoid Tumor (AT/RT) Arising From Ependymoma: A Type of AT/RT Secondarily Developing From Other Primary Central Nervous System Tumors. J Neuropathol Exp Neurol **2016**;75(2):167-74 doi 10.1093/jnen/nlv017.
34. Cachia D, Wani K, Penas-Prado M, Olar A, McCutcheon IE, Benjamin RS*, et al.* C11orf95-RELA fusion present in a primary supratentorial ependymoma and recurrent sarcoma. Brain Tumor Pathol **2015**;32(2):105-11 doi 10.1007/s10014-014-0205-1.
35. Sturm D, Orr BA, Toprak UH, Hovestadt V, Jones DTW, Capper D*, et al.* New Brain Tumor Entities Emerge from Molecular Classification of CNS-PNETs. Cell **2016**;164(5):1060-72 doi 10.1016/j.cell.2016.01.015.
36. Wu L, Sun T, Kobayashi K, Gao P, Griffin JD. Identification of a family of mastermind-like transcriptional coactivators for mammalian notch receptors. Mol Cell Biol **2002**;22(21):7688-700 doi 10.1128/mcb.22.21.7688-7700.2002.
37. Widera D, Mikenberg I, Elvers M, Kaltschmidt C, Kaltschmidt B. Tumor necrosis factor alpha triggers proliferation of adult neural stem cells via IKK/NF-kappaB signaling. BMC Neurosci **2006**;7:64 doi 10.1186/1471-2202-7-64.
38. Young KM, Bartlett PF, Coulson EJ. Neural progenitor number is regulated by nuclear factor-kappaB p65 and p50 subunit-dependent proliferation rather than cell survival. J Neurosci Res **2006**;83(1):39-49 doi 10.1002/jnr.20702.
39. Yang ZJ, Ellis T, Markant SL, Read TA, Kessler JD, Bourboulas M*, et al.* Medulloblastoma can be initiated by deletion of Patched in lineage-restricted progenitors or stem cells. Cancer Cell **2008**;14(2):135-45 doi 10.1016/j.ccr.2008.07.003.
40. Schuller U, Heine VM, Mao J, Kho AT, Dillon AK, Han YG*, et al.* Acquisition of granule neuron precursor identity is a critical determinant of progenitor cell competence to form Shh-induced medulloblastoma. Cancer Cell **2008**;14(2):123-34 doi 10.1016/j.ccr.2008.07.005.
41. Gojo J, Englinger B, Jiang L, Hübner JM, Shaw ML, Hack OA*, et al.* Single-Cell RNA-Seq Reveals Cellular Hierarchies and Impaired Developmental Trajectories in Pediatric

Ependymoma. Cancer Cell **2020**;38(1):44-59.e9 doi https://doi.org/10.1016/j.ccell.2020.06.004.

42. Wee S, Wiederschain D, Maira SM, Loo A, Miller C, deBeaumont R*, et al.* PTEN-deficient cancers depend on PIK3CB. Proc Natl Acad Sci U S A **2008**;105(35):13057-62 doi 10.1073/pnas.0802655105.
43. Wiederschain D, Wee S, Chen L, Loo A, Yang G, Huang A*, et al.* Single-vector inducible lentiviral RNAi system for oncology target validation. Cell Cycle **2009**;8(3):498-504 doi 10.4161/cc.8.3.7701.
44. Feng W, Herbst L, Lichter P, Pfister SM, Liu HK, Kawauchi D. CRISPR-mediated Loss of Function Analysis in Cerebellar Granule Cells Using In Utero Electroporation-based Gene Transfer. J Vis Exp **2018**(136) doi 10.3791/57311.
45. Feng W, Kawauchi D, Körkel-Qu H, Deng H, Serger E, Sieber L*, et al.* Chd7 is indispensable for mammalian brain development through activation of a neuronal differentiation programme. Nat Commun **2017**;8:14758 doi 10.1038/ncomms14758.
46. Huber W, Carey VJ, Gentleman R, Anders S, Carlson M, Carvalho BS*, et al.* Orchestrating high-throughput genomic analysis with Bioconductor. Nat Methods **2015**;12(2):115-21 doi 10.1038/nmeth.3252.
47. Aryee MJ, Jaffe AE, Corrada-Bravo H, Ladd-Acosta C, Feinberg AP, Hansen KD*, et al.* Minfi: a flexible and comprehensive Bioconductor package for the analysis of Infinium DNA methylation microarrays. Bioinformatics **2014**;30(10):1363-9 doi 10.1093/bioinformatics/btu049.
48. Campello RJGB, Moulavi D, Sander J. Density-Based Clustering Based on Hierarchical Density Estimates. Advances in Knowledge Discovery and Data Mining; 2013; Berlin, Heidelberg. Springer Berlin Heidelberg. p 160-72. (Advances in Knowledge Discovery and Data Mining).
49. Monti S, Tamayo P, Mesirov J, Golub T. Consensus Clustering: A Resampling-Based Method for Class Discovery and Visualization of Gene Expression Microarray Data. Machine Learning **2003**;52(1):91-118 doi 10.1023/A:1023949509487.
50. Sahm F, Schrimpf D, Jones DT, Meyer J, Kratz A, Reuss D*, et al.* Next-generation sequencing in routine brain tumor diagnostics enables an integrated diagnosis and identifies actionable targets. Acta Neuropathol **2016**;131(6):903-10 doi 10.1007/s00401-015-1519-8.
51. Sahm F, Schrimpf D, Stichel D, Jones DTW, Hielscher T, Schefzyk S*, et al.* DNA methylation-based classification and grading system for meningioma: a multicentre, retrospective analysis. The Lancet Oncology **2017**;18(5):682-94 doi https://doi.org/10.1016/S1470-2045(17)30155-9.
52. Okonechnikov K, Imai-Matsushima A, Paul L, Seitz A, Meyer TF, Garcia-Alcalde F. InFusion: Advancing Discovery of Fusion Genes and Chimeric Transcripts from Deep RNA-Sequencing Data. PLOS ONE **2016**;11(12):e0167417 doi 10.1371/journal.pone.0167417.
53. Ritchie ME, Phipson B, Wu D, Hu Y, Law CW, Shi W*, et al.* limma powers differential expression analyses for RNA-sequencing and microarray studies. Nucleic Acids Res **2015**;43(7):e47-e doi 10.1093/nar/gkv007.
54. Bindea G, Mlecnik B, Hackl H, Charoentong P, Tosolini M, Kirilovsky A*, et al.* ClueGO: a Cytoscape plug-in to decipher functionally grouped gene ontology and pathway annotation networks. Bioinformatics **2009**;25(8):1091-3 doi 10.1093/bioinformatics/btp101.

Figure Legends

Figure 1. Diagnostically ambiguous supratentorial ependymoma form discrete clusters.

A, Unsupervised clustering of reference cohort samples (n = 501 from two previous studies (5,6), additional non-reference samples (n = 507) and exploratory samples (n = 20) using t-SNE dimensionality reduction (5,6). **B,** t-SNE plot based on a hierarchical density-based clustering scan (HDBSCAN) comprising samples from cluster 1-4 and ST-EPN-RELA in A (n = 613). Respective calibrated classification scores based on the Heidelberg Brain Tumor Methylation Classifier, v11B4 are encoded red if ≥ 0.9 (= predicted as ST-EPN-RELA) or black if < 0.9 (= no assignment to any of the defined brain tumor methylation classes) (15). Samples classified as outlier by the HDBSCAN (n = 25) are marked with a black line. **C,** Copy number variations observed in the ST-EPN-RELA cluster and clusters 1-4 plotted as frequencies at which these aberrations occurred within respective clusters. Detailed aberrations per sample are given in Supplementary Table S1 and S2.

Figure 2. ST-EPN-RELA satellite clusters harbor alternative ZFTA fusion genes.

A, t-SNE for samples from clusters 1–4. Colors indicate respective fusion types. **B,** Visualization of the different fusion constructs containing *ZFTA* that were detected in the four satellite clusters. Detailed information on the different domains within the fusion construct of *ZFTA-CTNNA2* was not available due to the detection method (DNA-panel seq.). ZF = zinc finger domain, TAD= transactivation domain. **C,** Fusion plot summarizing fusion partners of *ZFTA* in the ST-EPN-RELA cluster and clusters 1-4 that were identified in samples with high confidence. Line width represents the frequency of detected fusion.

Figure 3. Tumors harboring alternative fusions exhibited a broad spectrum of institutionally determined histological diagnoses.

A, Oncoplot depicting DNA-methylation profiling results, reported histopathological diagnoses, detected gene fusions, structural variations typical for ST-EPN-RELA and methods/material used for the respective analyses for all samples of the four satellite clusters (n = 96). **B-E,** Examples for the highly variable histology of cases from the

satellite clusters: HE stainings (Scale bar = 200 µm) of tumors from cluster 2 (**B**, **C**; green frame) and cluster 3 (**D**, **E**; yellow frame). The upper cases (**B**, **D**) show typical perivascular pseudo-rosettes (highlighted in inset). The lower cases (**C**, **E**) lack these pseudo-rosettes and show extensive mesenchymal/fibrotic areas (**C**) or small cells, partially with peri-nuclear halos (**E**). **F-I,** IHC-staining illustrating the variable degree of L1CAM-positivity in cases from cluster 2 (**F**, **G**; green frame), cluster 3 (**H**; yellow frame), and cluster 4 (**I**; blue frame). L1CAM-expression ranges from negative (**F**) over weakly positive (**G, H**) to strongly positive (**I**). The detected fusion in each sample is given at the lower right. **J-M,** IHC-staining illustrating the variable degree of p65-positivity in cases from cluster 1 (**J**; orange frame), cluster 2 (**K**; green frame), and cluster 3 (**L**, **M**; yellow frame). p65-expression ranges from negative (**K**) over weakly positive (**L**, **M**) to strongly positive (**J**). The detected fusion in each sample is given at the bottom of micrographs.

Figure 4. ZFTA fusion genes exert their oncogenicity in the developing cerebral cortex via a distinct zinc finger domain.

A, Graphical illustration of the plasmid constructs used for modelling ST tumors in mice. All constructs are tagged with the human influenza hemagglutinin surface glycoprotein (HA). *ZFTA* or *ZFTA*-fusion constructs were cloned into the pT2K transposable vector and injected with the Tol2 transposase into the lateral ventricle of E13.5 wild-type mice followed by transfection using an electroporation-based *in vivo* gene transfer approach. CAG, CMV early enhancer/chicken beta actin promotor. IRES, internal ribosomal entry site. Tol2, Tol2 transposase cis element. **B,** Kaplan-Meier survival curves along with the numbers of surviving animals electroporated with *ZFTA* or indicated *ZFTA* fusion genes. Note that YAP1-MAMLD1 was used as a positive control. Log-rank test compares each ZFTA fusion to ZFTA wild-type. **C-F,** Micrographs (H&E) of ZFTA fusion-driven tumors in mice. (Scale bar = 300 µm and 50 µm for insets). **G-J,** Immunostaining using an anti-HA antibody on respective ZFTA fusion-driven tumors shown in **C-F** (Scale bar = 50 µm). **K,** *In vivo* bioluminescence images at weeks 1, 2 and 4 after birth of the electroporated animals. **L,** Kaplan-Meier survival curves of mice electroporated with *ZFTA-RELA* (that corresponds to 3B) and *ZFTA(ΔZF1)-RELA/MAML2/NCOA2* constructs. ***P < 0.001; ****P < 0.0001

Figure 5. ZFTA fusion-associated murine tumor models share molecular characteristics with human ST-EPN-RELA.

A and B, Principle component analysis in **A** and hierarchical clustering in **B** based on orthologous genes expressed in human ST-EPN-RELA (solid red) and ST-EPN-YAP1 (solid cyan) tumors and murine *ZFTA-RELA* (hollow red), *ZFTA-MAML2* (hollow green), *ZFTA-NCOA2* (hollow purple) and *YAP1-MAMLD1*-driven (hollow cyan) tumors. Each dot represents one tumor. **C,** Expression level of *Ccnd1/CCND1* in mouse (left) and in human (right); ****P < 0.0001. **D,** Expression level of *L1cam/L1CAM* in mouse (left) and in human (right); ns, nonsignificant; *P < 0.0332; ****P < 0.0001.

Figure 6. Cross-species analysis identifies putative downstream oncogenes.

A, Schematic representation of cross-species analysis using Affymetrix gene expression data from human ST-EPN-RELA vs. all other EPNs (left column) and Affymetrix gene expression data (430V2 chip) from ZFTA fusion-driven murine models vs. YAP1-MAMLD1-driven murine model (right column); extraction of 535 orthologous genes commonly activated in human and mouse ZFTA-driven tumors (bottom). **B,** Heatmap of the 32 genes implicated in cancer-related signaling pathways as extracted from gene ontology (GO) analysis. **C-E,** ChIP-seq and CUT&RUN using HA-directed or H3K27ac antibodies and ATAC-seq in murine ZFTA-RELA-HA fusion-induced tumors reveals binding at *Gli2* (**C**)*,2 Lef1* (**D**) and *Ephb2* (**E**). Integration with previously published data on regulatory elements indicates active enhancers in human ST-EPN-RELA (22). IgG was used to control for non-specific signaling.

Figure 7. Gli2 is a downstream gene of ZFTA fusion-driven oncogenic signaling.

A, Illustration of the plasmid vector carrying *ZFTA-RELA* fused to the genes encoding a dominant-negative form of indicated oncoproteins with T2A self-cleaving peptides. **B,** Kaplan-Meier survival curves of mice electroporated with *ZFTA-RELA* (median survival = 44 days) or *ZFTA-RELA-T2A-dnGli2* (solid line), *-dnEphb2* (dashed line, median survival = 36 days), *-dnLef1* (dotted line, median survival = 20 days) constructs. ****P < 0.0001, *P = 0.0201, ns = non-significant **C,** *In vivo* bioluminescence images at week 1-4 after birth of animals electroporated with indicated constructs. **D,** Transcription factor enrichment analysis of GLI2 within histone H3K27Ac-marked enhancers across human primary ST-EPNs and PF-EPNs. **E,** Relative expression of GLI2 at mRNA level in the EP1NS cell line 48h after dox-treatment inducing shGLI2

expression. P value determined by paired t test. shGLI2_1: n = 4, mean = 0.6529, SD = 0.07702, P = 0.0041; shGLI2_2: n = 4, mean = 0.6137, SD = 0.1887, P = 0.0465. shControl: n = 4, mean = 1.076, SD = 0.134. **F**, Relative level of EdU (red dots) and Annexin V (blue dots) in EP1NS cell line 96h after dox-treatment compared to the ones without dox-treatment. P value determined by paired t test. For EdU: shGLI2_1: n = 6, mean = 72.17%, SD = 7.627, P < 0.0001; shGLI2_2: n = 6, mean = 76.33%, SD = 3.983, P = 0.0009; shControl: n = 6, mean = 98.5%, SD = 7.530. For Annexin V: shGLI2_1: n = 6, mean = 113.5%, SD = 10.86, P = 0.0251; shGLI2_2: n = 6, mean = 127.5%, SD = 16.06, P = 0.0223; shControl: n = 6, mean = 94.67%, SD = 12.36. **G**, The Kaplan-Meier curves of the electroporated mice treated with ATO (blue curve, median survival = 36 days) or vehicle (black curve, median survival = 13 days). P value determined by Log-rank test (P = 0.0104). All error bars represent standard deviation (SD). ****P < 0.0001, *** P < 0.001, **P < 0.01, *P < 0.05.

Figure 1

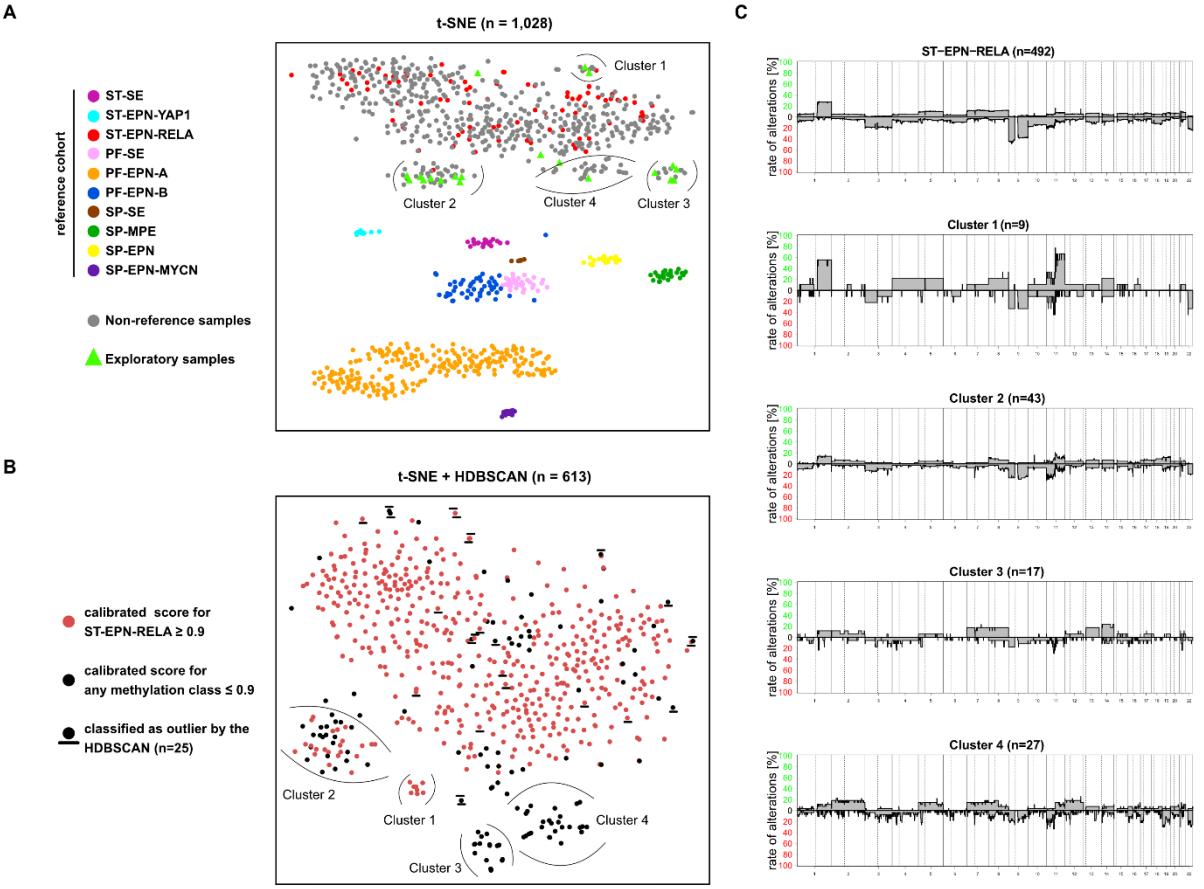

Author Manuscript Published OnlineFirst on April 20, 2021; DOI: 10.1158/2159-8290.CD-20-0963
Author manuscripts have been peer reviewed and accepted for publication but have not yet been edited.

Figure 2

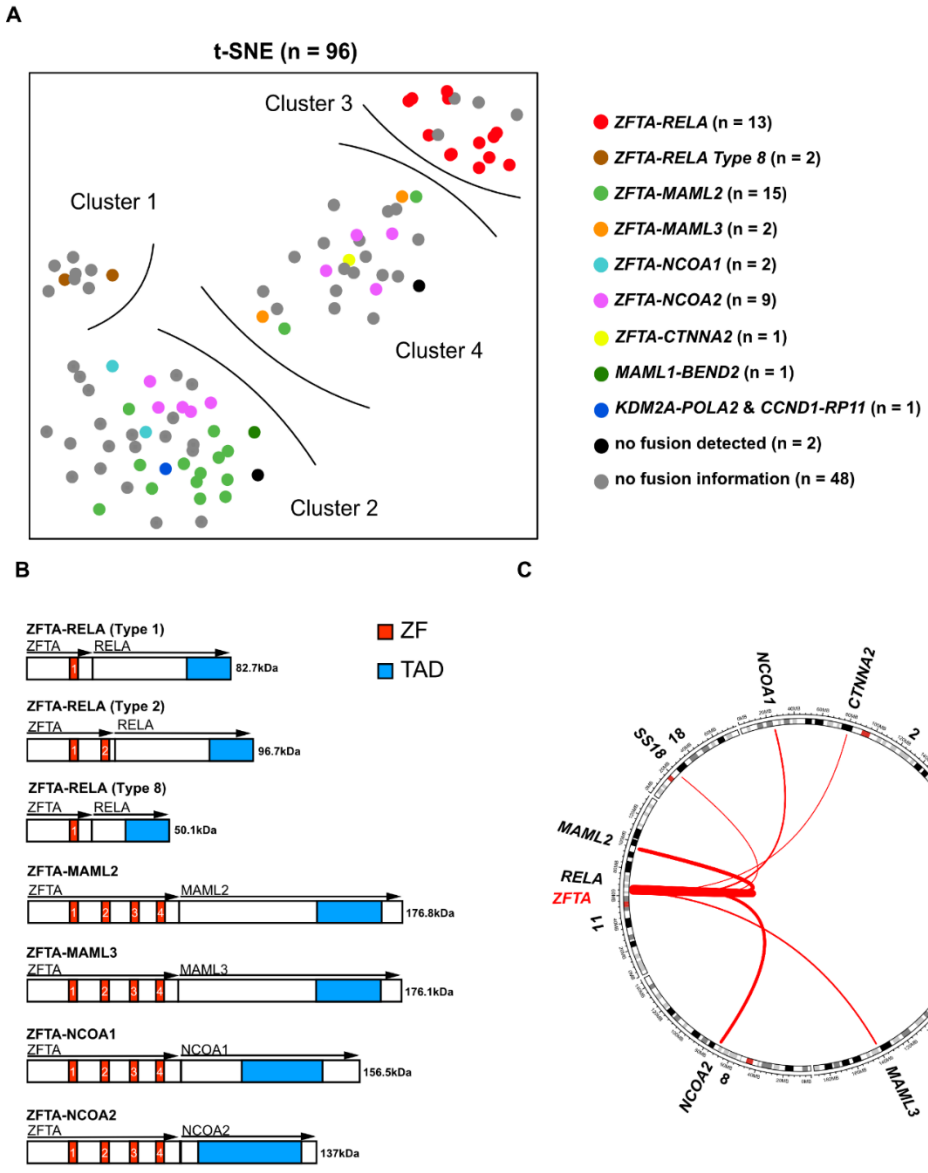

Author Manuscript Published OnlineFirst on April 20, 2021; DOI: 10.1158/2159-8290.CD-20-0963
Author manuscripts have been peer reviewed and accepted for publication but have not yet been edited.

Figure 3

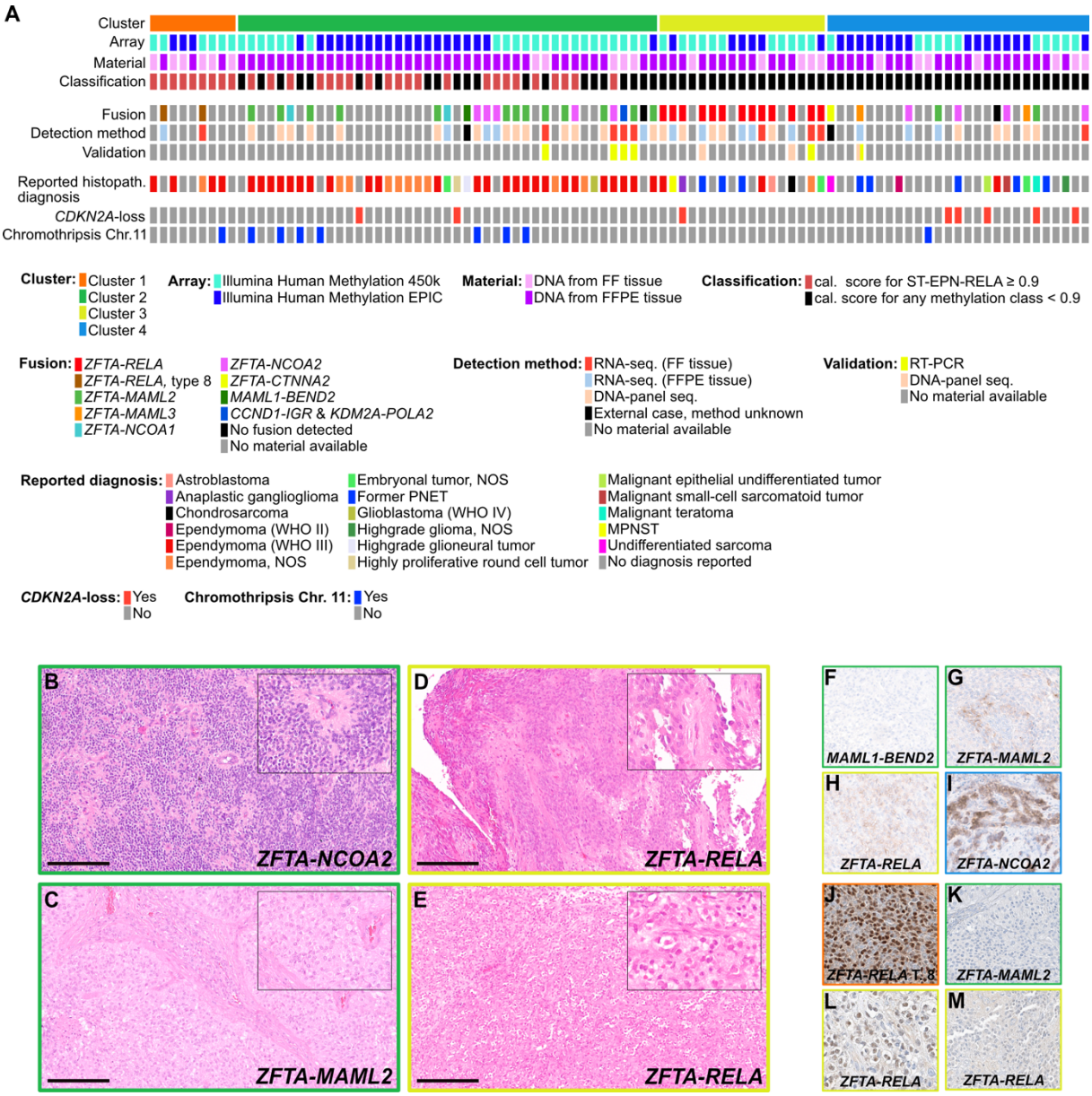

Author Manuscript Published OnlineFirst on April 20, 2021; DOI: 10.1158/2159-8290.CD-20-0963
Author manuscripts have been peer reviewed and accepted for publication but have not yet been edited.

Figure 4

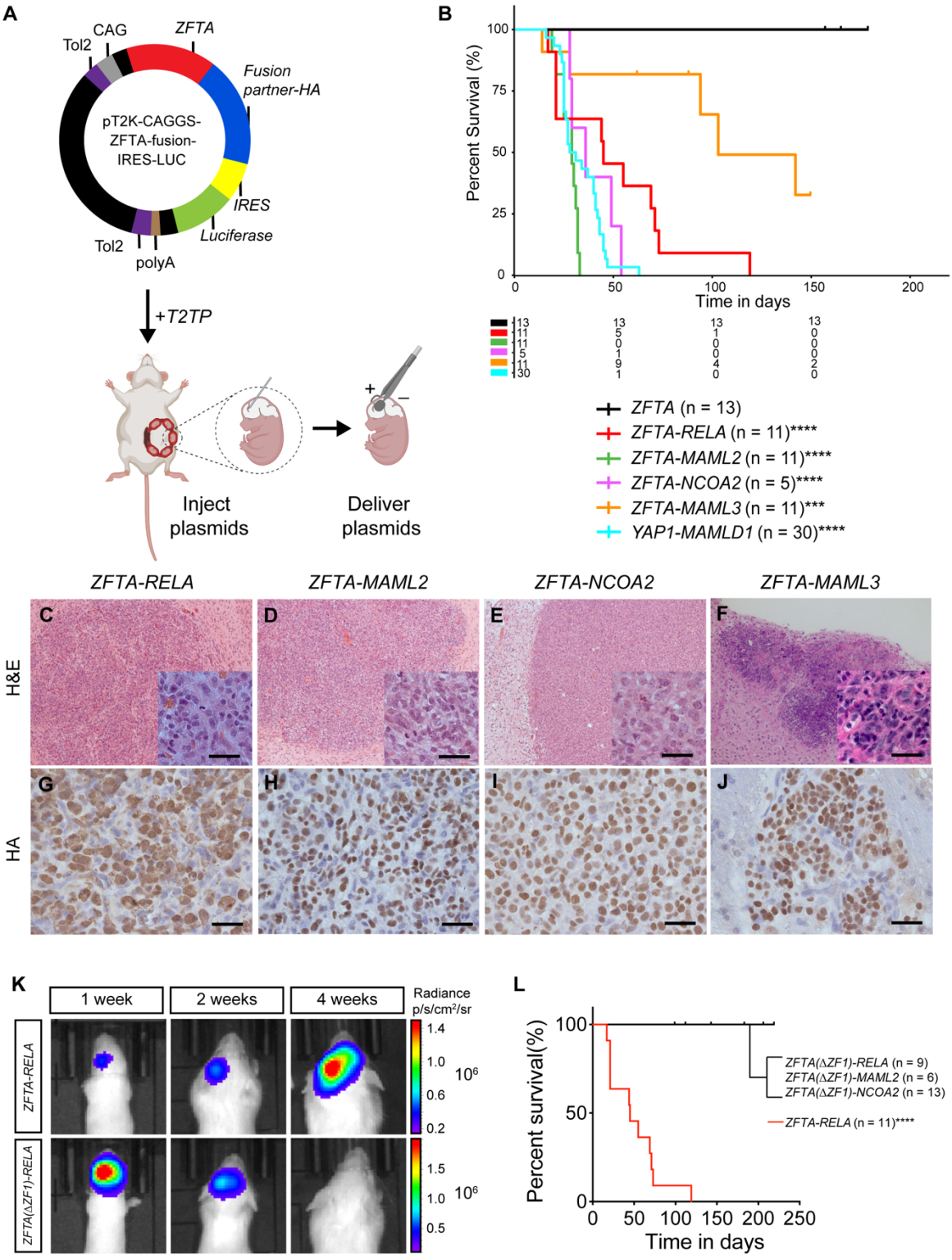

Author Manuscript Published OnlineFirst on April 20, 2021; DOI: 10.1158/2159-8290.CD-20-0963
Author manuscripts have been peer reviewed and accepted for publication but have not yet been edited.

Figure 5

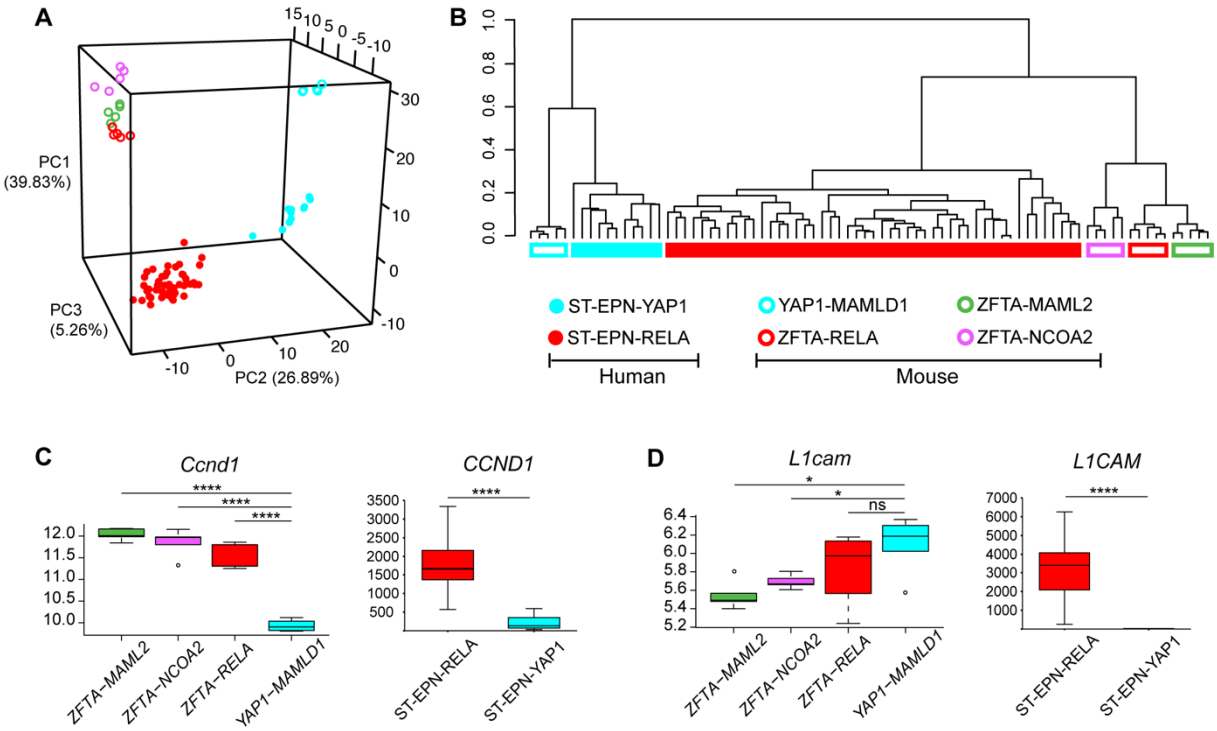

Author Manuscript Published OnlineFirst on April 20, 2021; DOI: 10.1158/2159-8290.CD-20-0963
Author manuscripts have been peer reviewed and accepted for publication but have not yet been edited.

Figure 6

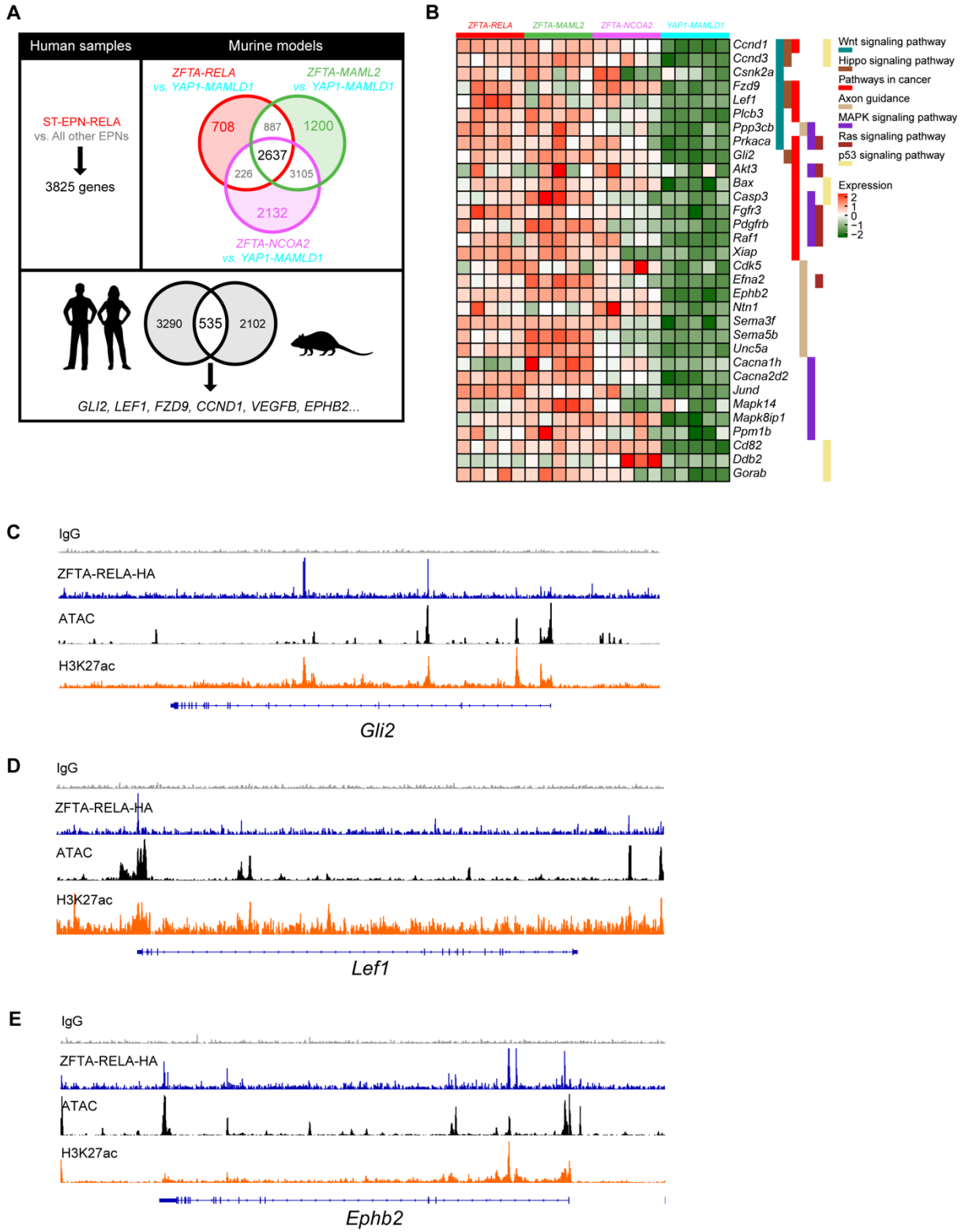

Author Manuscript Published OnlineFirst on April 20, 2021; DOI: 10.1158/2159-8290.CD-20-0963
Author manuscripts have been peer reviewed and accepted for publication but have not yet been edited.

Figure 7

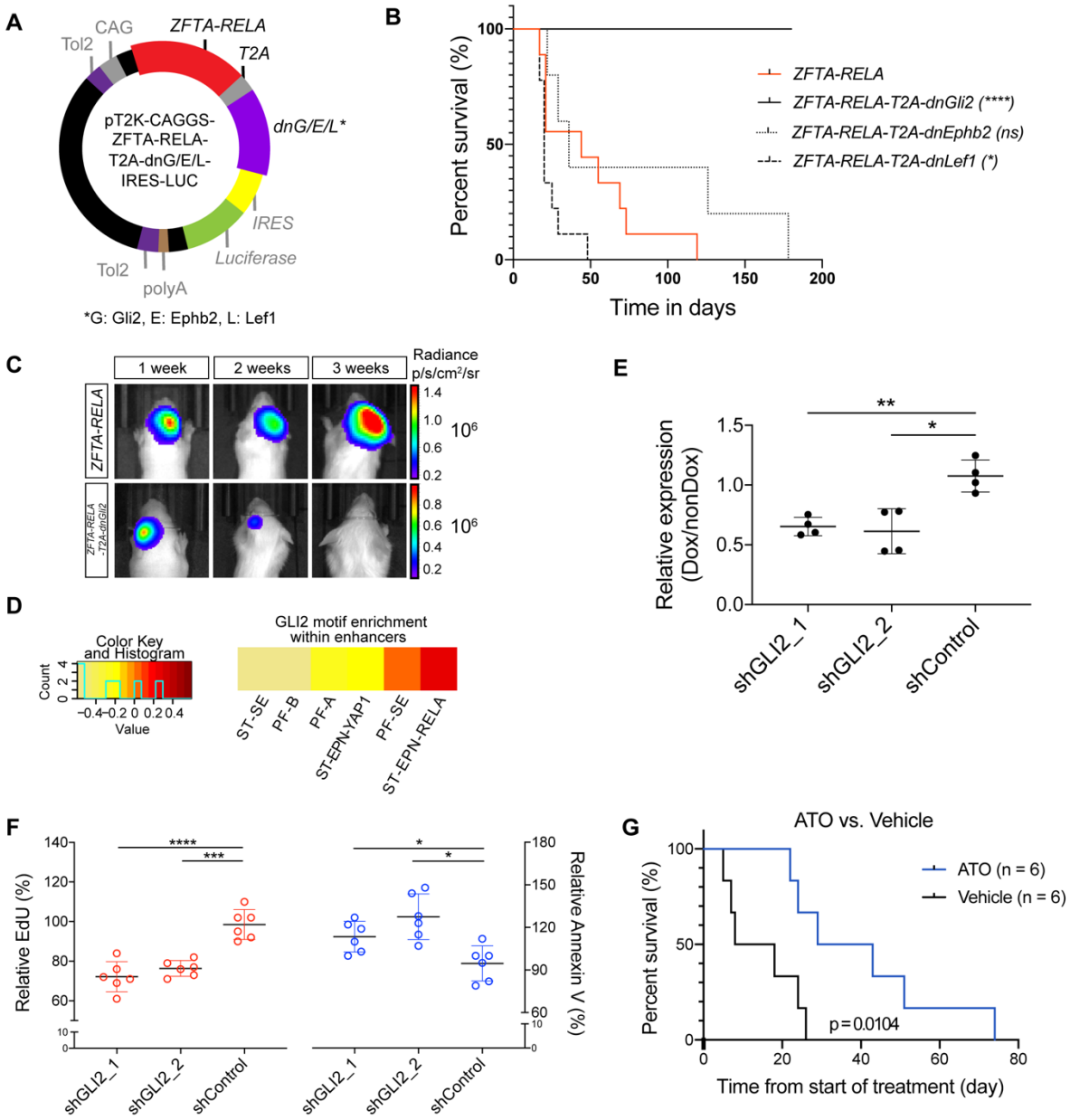

AACR American Association for Cancer Research

CANCER DISCOVERY

Cross-species genomics reveals oncogenic dependencies in ZFTA/C11orf95 fusion-positive supratentorial ependymomas

Tuyu Zheng, David R. Ghasemi, Konstantin Okonechnikov, et al.

Cancer Discov Published OnlineFirst April 20, 2021.